8-2007

Mixed Quantum-Classical Molecular Dynamics Study of a Hydrated Electron and an Investigation of Temperature Control Algorithms

Janet Aremu-cole
Clemson University, Jaremuc@clemson.edu

MIXED QUANTUM-CLASSICAL STUDY OF A HYDRATED ELECTRON AND INVESTGATION OF TEMPERATURE-CONTROL ALGORITHMS

A Dissertation
Presented to
the Graduate School of
Clemson University

In Partial Fulfillment
of the Requirements for the Degree
Doctor of Philosophy
Chemistry

---

by
Janet Eyiwumi Aremu-Cole
August 2007

Accepted by:
Dr. Steven Stuart, Committee Chair
Dr. Jason McNeil
Dr. Brian Dominy
Dr. Robert Latour

ABSTRACT

The use of classical and quantum mechanics has been employed in this dissertation to study temperature control algorithms and a hydrated electron. A comparison of the effects of four commonly used temperature control algorithms on the energetics and dynamics of liquid water has been executed, in efforts to better understand the non-equipartitioning effects caused by some thermostats. The Berendsen, Andersen, Langevin, and velocity rescaling temperature control algorithms were applied to both dimer and bulk water systems, using the TIP4P water model. The two deterministic thermostats, Berendsen and velocity rescaling, display the "flying ice cube effect" that had been noticed earlier for the velocity rescaling thermostat (S.C. Harvey et al, *J. Comp. Chem.* **19**, 727 (1998)). Specifically, these thermostats lead to violation of energy equipartition, with the rotational temperature much colder and the translational temperature much hotter than the mean temperature. The two stochastic thermostats, on the other hand, Andersen and Langevin, both lead to correct, equilibrium equipartitioning of the system energy. The computational details and simulation results are discussed in Chapter 2, and specific thermostat algorithms are discussed in Chapter 1, Section 1.1.

The effects of different water models on the physical properties of a hydrated electron have been studied. Prior simulation studies have been performed primarily with the SPC-FLEX water model, and have resulted in only partial agreement with experiment. Consequently, it is of considerable interest to determine whether the choice of water model has a large effect on the properties

of the hydrated electron. Properties such as the energy of the ground state wavefunction, radius of gyration of the electron, and the absorption spectrum were calculated from adiabatic dynamics simulations of a single electron hydrated by SPC, TIP4P and TIP4P-FQ water. We observed that the choice of water model significantly affects the energetics and dynamics of the hydrated electron. We also found that the absorption spectra of the hydrated electron solvated in both polarizable and nonpolarizable water using the Rossky electron water Pseudopotential, continues to be blue-shifted. The computational details and simulation results are discussed in Chapter 3, and Chapter 4.

DEDICATION

I would like to dedicate my dissertation to God, who endowed me with the ability and strength I needed to complete this task; my son David Floyd, parents Yetunde and James Aremu-Cole and husband Chris Floyd; my best friends Dianne Hogan-Thrower, Esther Onyoni, and Fatimah Oloriegbe; my God-sent guardian angels: Michelle Richardson and Marcia Noad.

I would like to say thank you to all of you, from the bottom of my heart.

ACKNOWLEDGMENTS

I would like to acknowledge my advisor Dr. Steven Stuart for his dedication and patience; my group members both current and past: Yang Li, Suleiman Oloriegbe, Todd Knippenberg, and Michael Mury.

Finally, my cheerleaders, I want to say a big thank you! Mrs. Felicia Ogunsile, Fatimah Oloriegbe, Toyin Aremu-Cole, Mo, and Kimberly Poole. I thank God for you all.

TABLE OF CONTENTS

LIST OF TABLES

LIST OF FIGURES

List of Figures (Continued)

CHAPTER ONE
INTRODUCTION

Computational chemistry, also known as molecular modeling, is a branch of chemistry that uses computer algorithms based on mathematical expressions from theoretical chemistry, to study matter. Computational chemistry has become a very vital tool in acquiring information that gives better insight into both the physical and chemical properties of materials. Computational studies have been applied to various aspects of chemistry such as the prediction of reaction mechanisms, calculation of rate constants, elucidation of spectroscopic data, and prediction of molecular geometry and structure.

Computational chemistry methods and algorithms can be divided into six main classes: molecular dynamics algorithms[1-3], molecular mechanics algorithms[4, 5], Monte Carlo algorithms[6, 7], ab initio calculations[8-11], semi-empirical calculations, and density functional calculations[12, 13]. Ab initio calculations, semi-empirical calculations, and density functional calculations are all governed by quantum mechanics in their problem solving approach. Molecular mechanics algorithms, classical molecular dynamics algorithms (CMD), and Monte Carlo algorithms are governed by classical mechanics; therefore they do not provide electronic information. The work described in this dissertation uses both classical and quantum mechanical approaches to study properties of water and solvated electrons.

Molecular dynamics allows computational chemists to study the motion, i.e. the dynamics, of atoms or molecules over time. CMD is also used to study

large systems and in comparison to methods based on solving Schrödinger's equation, molecular dynamics is computationally less expensive.

Molecular mechanics is an algorithm that uses force fields to calculate conformational energy associated with a molecular geometry. Molecular mechanics calculates conformational energy without accounting for thermal fluctuations. Well known programs such as AMBER[14] and CHARMM[15] employ the use of molecular mechanics and dynamics.

The Monte Carlo (MC) algorithm differs from molecular dynamics and mechanics because it employs the use of random walks to generate new positions for atomic sites during the course of a simulation. With MC, an acceptance criterion is built into the cycle of events, and this criterion determines whether a move is accepted or rejected. After a move is accepted energies associated with the new configuration are calculated and equilibrium thermodynamic data can be acquired.

Ab initio calculations are based on solving Schrödinger's equation. Using ab initio calculations, details about electronic properties (*i.e.* electronic energies, and wavefunctions) can be obtained. Since the solutions to the electronic Schrödinger's equation for complex systems cannot be solved exactly, and are computationally expensive, ab initio calculations are typically applied to very small systems.

Semi-empirical calculation, as the name implies, is a mixing of theory and experimentally obtained data. It is based on the Hatree Fock formalism[16], but it employs the use of approximations and empirical data in solving complicated

integrals. Semi-empirical calculations typically neglect two-electron integrals and are parameterized using empirical data. These types of simulations allow the study of large molecules with inclusion of few or no correlation effects.

Density functional theory is also based on Schrödinger's equation, but unlike semi-empirical and ab initio methods it does not represent the system in terms of wavefunctions. Instead, the system is represented by the electron density. The premise of DFT is in finding the electron density that gives the minimum ground state energy.

In our studies the use of molecular dynamics and ab-initio calculations has been employed. In Chapter 2, molecular dynamics was used in an investigation of temperature control algorithms, and in Chapters 3 and 4, we used mixed quantum-classical molecular dynamics, including single electron Hartree-Fock calculations, to study the structure, energetics and dynamical properties of a hydrated electron. In the following Chapters is a detailed presentation of these studies.

In the study of temperature control algorithms, we applied four commonly used algorithms: the Andersen[17], Berendsen[18], Langevin[1] and velocity rescaling algorithms, to maintain the temperature of liquid water. The effect of each thermostat on the dynamics of the water molecules and the distribution of energies between various degrees of freedom has been explored. Details of our temperature control algorithm study are covered in Chapter two.

In the second part of this dissertation we employ the use of mixed quantum-classical molecular dynamics to study a hydrated electron. The hydrated

electron is treated within the Born-Oppenheimer approximation[19] and in the adiabatic limit. The electron is treated as a quantum mechanical solute, and the water molecules are treated as classical particles. The motions of the atoms and molecules are governed by Newtonian mechanics. In this study the effects of water model geometry and polarization are explored, and details are covered in Chapters three and four.

1.1 Classical Molecular Dynamics

Classical molecular dynamics[1, 2] is an atomistic simulation algorithm in which every atom or molecule in the specified system is governed by Newtonian mechanics and electronic degrees of freedom are unaccounted for. Classical molecular dynamics is an excellent tool for studying the motions and structure of molecules over time. Classical molecular dynamics simulations have been applied to a number of investigations, including protein folding studies, formation of carbon nanotubes, thermal degradation in aromatic polymers and drug design.

Alder and Wainwright first introduced this method in the 1950's[3]. They invented CMD to help study the interactions of hard spheres. In 1974 the method was extended[20], and applied to the study of realistic solvents such as liquid water. McCammon et al., in 1977 performed the first CMD simulation of a biological system[21]. Since then, the use of CMD to study molecular interactions has expanded, and it is being applied to very complex systems.

Classical molecular dynamics simulations give thermodynamic information about a system, by converting microscopic information via statistical

mechanics[22]. Statistical mechanics provides the mathematical expressions that allows us to relate thermodynamic information such as pressure, and kinetic and potential energies, to microscopic data such as positions and velocities of atoms[22, 23]. Time-independent statistical averages are used in order to link thermodynamic data to microscopic data. These statistical averages, also known as ensemble averages, are taken over many data points. There are several different ensembles in which these averages maybe evaluated: the microcanonical, canonical, isobaric-isothermal, isoenthalpic-isobaric, grand-microcanonical, grand isothermal-isobaric, generalized and grand-canonical ensembles and many more. Each ensemble is characterized by certain thermodynamic properties that are fixed in that ensemble. Refer to Table 1.1.

Ensembles	**Fixed Properties**		
Microcanonical	N	V	E
Canonical	N	V	T
Grand - Canonical	μ	V	T
Isothermal isobaric	N	T	P
Isoenthalpic isobaric	N	H	P
Grand - Microcanonical	μ	V	E
Generalized	μ	P	T

Table 1.1: Characterization of seven commonly used ensembles. Each ensemble describes a specific type of macroscopic system. The fixed properties that describe each ensemble are defined as follows: N = number of atoms, V = volume, E = energy, T = temperature, μ = chemical potential, P = pressure and H = enthalpy.

Prior to performing a CMD simulation, a determination is made as to which ensemble is required and this determination is made based on the type of physical system that is going to be considered. In a study where experimental conditions are critical, and temperature is controlled in the experiment, an ensemble such as the canonical ensemble would be required to reproduce the experimental conditions. In order to work within ensembles such as the canonical ensemble where temperature is fixed, a temperature control algorithm is needed. There are several different types of temperature control algorithms that can be used during the course of a CMD simulation.

Temperature Control Algorithms

Temperature control algorithms, also known as thermostats, allow the temperature of a system to be maintained during the course of a CMD simulation. The use of thermostats allows scientists to study phenomena that are temperature dependent, such as heat flow in a non-equilibrium system, and minimize energy drifts associated with accumulation of numerical errors.

In our study we selected four commonly used thermostats, and applied them to constraining the temperature of bulk water over an extended period of time. The four thermostats chosen are the velocity rescaling, Andersen[17], Langevin[1, 18], and Berendsen[17] thermostats.

A. Velocity Rescaling Thermostat and Temperature Calculations

The velocity rescaling algorithm is the most basic approach to constraining temperature in an MD simulation. As the name suggests, this algorithm operates by uniformly rescaling the atomic velocities by a factor γ. This factor,

$$\gamma = \sqrt{\frac{T_o}{T}}, \qquad (1)$$

is chosen such that when all velocities are scaled by γ, the system temperature T (which is proportional to the kinetic energy, and thus the sum of the squared velocities) is corrected to agree with the target temperature, T_0. These rescalings can occur at regular intervals, or every time the temperature differs by more than a specified deviation from the reference temperature. The system temperature used to make this decision and in the calculation of γ can be the instantaneous temperature, or it can be an average temperature, obtained as a time average over instantaneous velocities.

Because this algorithm completely prohibits temperatures (kinetic energies) outside of the specified range, it does not generate a canonical ensemble (which would have an unbounded, Maxwell-Boltzmann distribution of atomic velocities). The velocity rescaling thermostat is completely deterministic, meaning that the trajectory follows uniquely from the starting phase point. But the memory of the prior velocities is lost after each velocity rescaling, and the algorithm gives rise to irreversible dynamics. Also, due to the abrupt changes in the atomic velocities upon rescaling, the phase space trajectories are discontinuous.

B. Andersen Thermostat

The Andersen thermostat is a stochastic temperature control algorithm that replaces the velocities of selected atoms in the simulated system with new velocities drawn from a Maxwell-Boltzmann distribution at the desired temperature[17]. The atoms in the system may be thought of as being coupled to an Andersen heat bath; sporadic collisions with the bath generate Gaussian atomic velocities. In between collisions, the atoms evolve in the microcanonical ensemble. When an atom, *i*, is selected for rescaling, its velocity is determined randomly using a Maxwell-Boltzmann distribution probability,

$$p(v_i) = \left(\frac{m_i}{2\pi kT} \right)^{1/2} e^{-\frac{1}{2} m_i v_i^2 \Big/ kT}, \qquad (2)$$

where v_i represents one of the three Cartesian components of the velocity of atom *i* and m_i represents its mass.

Collisions with the Andersen heat bath can occur only for selected atoms, or for the entire system in a single timestep. The collisions can occur at regular intervals, or they may be Poisson distributed, so that the time τ between collisions obeys

$$p(\tau) = \alpha e^{-\alpha \tau}, \qquad (3)$$

with an average time between collisions of 1/α.

The Andersen thermostat is stochastic, rather than deterministic. That is, a number of different trajectories could result from the same initial state, because of the randomly chosen velocities. Because of the abrupt, instantaneous changes in velocities, the Andersen thermostat generates irreversible and discontinuous phase

space trajectories. However, because the velocities are always Boltzmann-distributed, the system state is sampled correctly from the canonical ensemble as long as the reassignment frequency is nonzero. The dynamics are physically realistic only in the microcanonical sections of the trajectory; if the reassignment frequency is small, much of the dynamics are physically realistic, but the dynamics of the velocity reassignment do not correspond to any real physical process.

C. Langevin Thermostat

The Langevin thermostat is another stochastic temperature control algorithm in which the atoms interact with a random heat bath. This thermostat is based on Langevin's equation of motion[24],

$$m_i a_i = F_i - \xi m_i v_i + R_i . \qquad (4)$$

The acceleration of atom i, a_i, is determined not only by the interatomic forces, as in Newton's equation of motion, but includes a random force R_i from collision with a heat bath, along with a friction force proportional to the atomic velocity and a friction coefficient, ξ. This friction coefficient can be chosen with physical input from the phonon frequencies in the substance of interest, but is more commonly chosen arbitrarily, especially for non-crystalline systems. The inverse of the friction coefficient defines a characteristic timescale with which the system temperature will approach the target temperature. The random or stochastic force, R_i, models thermal fluctuations in the bath, and is selected

randomly from a Gaussian distribution. This width of this distribution, chosen so as to satisfy the fluctuation-dissipation theorem,[25] is

$$\sigma = \sqrt{2 m_i k T_0 \xi dt}\,, \tag{5}$$

where *dt* is the simulation timestep.

Because the perturbations to the dynamics occur via the force, the phase space trajectories that are generated are continuous. The Langevin thermostat is stochastic, and thus generates trajectories that are not time-reversible. These trajectories do sample the canonical distribution, however.

D. Berendsen Thermostat

The Berendsen thermostat, like velocity rescaling, is a deterministic thermostat that perturbs the system velocities based on the current system temperature. It differs from velocity rescaling in that the adjustment required to bring the system temperature to the target value is not performed in a single step, but via a series of smaller adjustments[18, 26]. These adjustments can be made directly to the atomic velocities, in which case the algorithm resembles a "partial" velocity rescaling algorithm. Alternatively, the adjustments can be made via the atomic forces, preserving a continuous phase space trajectory. In this implementation, the equation of motion includes a frictional force,

$$a_i = \frac{F_i}{m_i} + \xi \zeta v_i\,, \tag{6}$$

where the scaling factor ,

$$\zeta = \left(\frac{T_0}{T} - 1 \right), \tag{7}$$

can give rise to a negative effective friction coefficient (viscous heating) when the instantaneous temperature T is lower than the target temperature T_0.

The Berendsen thermostat is deterministic, and gives rise to continuous phase space trajectories, but it does not generate the canonical ensemble, and it is time irreversible.

For any CMD simulation, once the choice of a temperature control algorithm has been made, initial positions and velocities for all the atoms in the system must be specified. Figure 1.1 presents a detailed representation of what happens during the course of a CMD simulation.

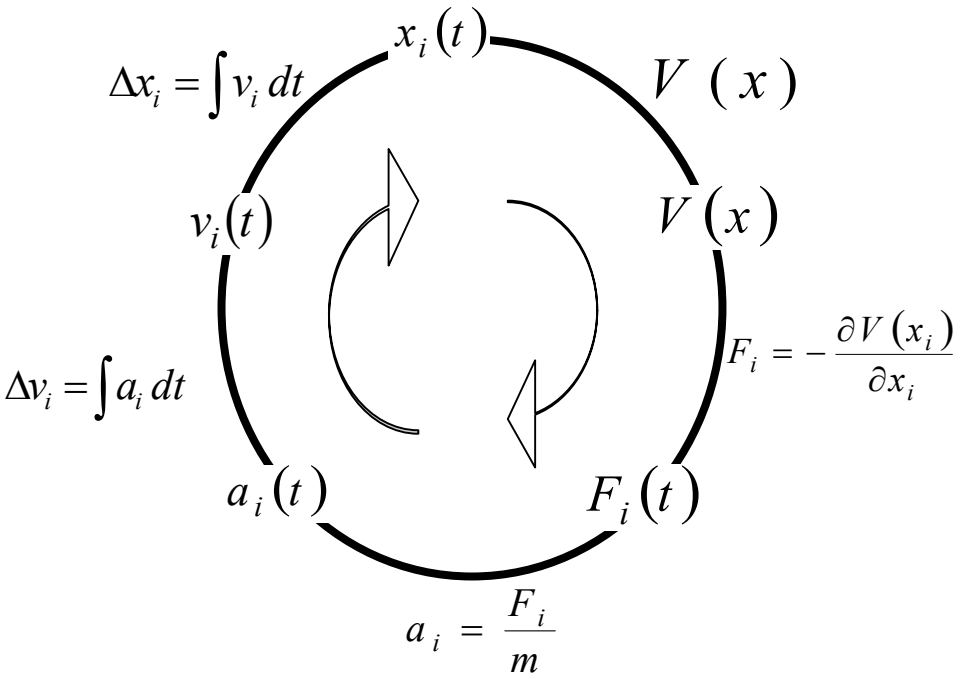

Figure 1.1: Illustration of the processes that occur during a classical molecular dynamics simulation. Positions, velocities and accelerations of each atom in the simulated system is represented by $x_i(t)$, $v_i(t)$ and $a_i(t)$, respectively. The potential energy, $V(x)$, describes the interatomic and intra-atomic interactions within the system. The forces, $F_i(t)$ are calculated from the gradient of the potential, $V(x)$.

The initial positions x_i(t) are specified, and then the interatomic and intra-atomic forces are calculated using the negative gradient of the potential, *V(x)*, which is a function of the positions. After the forces have been determined, accelerations are calculated using Newton's equation where $F_i = m_i a_i$.

Using common integrators such as the predictor-corrector algorithm[27], or Verlet algorithms,[28, 29] new velocities and positions are generated by integrating the accelerations. In our simulations, we use the velocity Verlet integrator to advance the positions and velocities of our atoms. The following equations represent the velocity Verlet integrator algorithm.

$$\dot{r}_i\left(t + \frac{1}{2}\delta t\right) = \dot{r}_i(t) + \frac{1}{2}\delta t \ddot{r}_i(t) \qquad (8)$$

$$r_i(t + \delta t) = \dot{r}_i(t) + \delta t \dot{r}_i(t) + \frac{1}{2}\delta t^2 \ddot{r}_i(t) \qquad (9)$$

$$\dot{r}_i(t + \delta t) = \dot{r}_i\left(t + \frac{1}{2}\delta t\right) + \frac{1}{2}\delta t \ddot{r}(t + \delta t) \qquad (10)$$

The atomic and molecular velocities are represented by $\dot{r}_i$, the timestep is represented by δt, acceleration is represented by $\ddot{r}$, and r_i represents the position of atoms in the system.

Classical molecular dynamics allows us to observe and study the motions of atoms over time. The time interval is broken up into increments referred to as time-steps. At every time-step, the CMD cycle is initiated and completed.

Classical molecular dynamics is based on two main approximations. Classical molecular dynamics works within the Born-Oppenheimer

approximation, and atomic motions are confined to a single potential energy surface.

The second consideration in CMD is that the atomic motions are governed by classical mechanics. Classical molecular dynamics is not sufficient to describe quantum mechanical processes such as electron transfer, and quantum mechanical tunneling. Mixed quantum-classical molecular dynamics described in Section 1.3, has been developed to help address some shortcomings of classical molecular dynamics.

1.2 Quantum Mechanics

Quantum mechanics is a more fundamental science than classical mechanics, because it allows us to study the world at a sub-atomic level. The foundations of quantum mechanics can be found in the works of renowned scientists such as Max Planck, Wolfgang Pauli, Erwin Schrödinger, Max Born, Paul Dirac, Albert Einstein, and Werner Heisenberg[30-32].

From quantum mechanics we have learned that light and matter exist as particles[32, 33]. Particles are represented by wavefunctions. Wavefunctions are an abstract mathematical construct that allows us to describe the state of any physical system. Wavefunctions have a probabilistic interpretation; therefore they can be used to calculate the probability of finding a particle at any given time and in any particular region.

The evolution of wavefunctions is described by Schrödinger's equation[34]

$$\hat{H}\Psi = E\Psi , \qquad (11)$$

where $\Psi(r_1, r_2, \ldots, t)$ is the wavefunction, that fully describes the state of any given system. The Hamiltonian operator, $\hat{H}$, is the quantum mechanical operator corresponding to the total energy of the system. Positions and time are represented by *r*, and *t*, respectively.

The system evolves in space and time according to Schrödinger's equation (SE), and the Hamiltonian operator for both the time-independent and time-dependent SE is defined as follows,

$$\hat{H}\,\psi\left(r,t\right) = i\hbar\,\frac{\partial\,\psi\left(r,t\right)}{\partial t}\,. \qquad (12)$$

Planck's constant is represented by $\hbar$ and *i* represents an imaginary unit.

Schrödinger's equation can be separated into the space and time components. This separation is plausible provided that the potential energy, *V(r)*, is independent of time. Using a technique known as separation of variables[32], we can solve Schrödinger 's equation and obtain two equivalent equations. The two equations obtained are shown in equations (13) and (14),

$$-\frac{\hbar^2}{2m}\frac{\partial^2\psi(r)}{\partial r^2} + V(r)\psi(r) = E\psi(r), \qquad (13)$$

$$i\hbar\frac{\partial\theta}{\partial t} = E\theta \text{ and } \theta = e^{\frac{-Et}{i\hbar}}\,. \qquad (14)$$

Equation (13) represents the time-independent formulation of Schrödinger's equation and equation (14) is the time-dependent version. There are other commonly used mathematically equivalent formulations of quantum mechanics apart from Schrödinger's wave mechanics. Heisenberg introduced the

use of matrix mechanics, and Paul Dirac combined wave mechanics and matrix mechanics to formulate what is now referred to as the Dirac bra-ket notation[31, 35].

Born-Oppenheimer Approximation

The Hamiltonian operator, $\hat{H}$, for a system of nuclei and electrons described by positions R_A and r_i, respectively, is described by the following equation

$$\hat{H} = -\frac{\hbar^2}{2m_e}\sum_{i}^{N}\nabla_i^2 - \frac{\hbar^2}{2}\sum_{A=1}^{M}\frac{1}{M_A}\nabla_A^2 - \sum_{i=1}^{N}\sum_{A=1}^{M}\frac{Z_A q_e^2}{r_{iA}} + \sum_{i=1}^{N}\sum_{j>i}^{N}\frac{q_e^2}{r_{ij}} + \sum_{A=1}^{M}\sum_{B>A}^{M}\frac{Z_A Z_B q_e^2}{R_{AB}}, \quad (15)$$

where *A, B,* represent the nuclei and *i, j,* represent the electrons[35]. The first term corresponds to the kinetic energy of the electrons, the second term represents the kinetic energy of the nuclei, and the third term represents the potential energy of the attraction between the nuclei and electrons. The potential energy of the repulsion between electrons is represented by the fourth term, and the fifth term represents the repulsion between the nuclei. The mass of an electron is defined as m_e, q_e represents charges, and Z represents atomic numbers. The Laplacian operator ∇^2, is defined as,

$$\nabla^2 = \frac{\partial^2}{\partial x^2} + \frac{\partial^2}{\partial y^2} + \frac{\partial^2}{\partial z^2} \quad . \quad (16)$$

The Born-Oppenheimer approximation is an approximation that has been employed in physics and chemistry, to help separate the motions of nuclei and electrons. In this approximation the terms corresponding to the nuclei and electronic coordinates in Schrödinger's equation are decoupled, and only the electronic terms are retained. This separation is valid because atomic nuclei are

much heavier than electrons and therefore move on a much slower timescale. The resulting equation after separating the motion of the nuclei and electrons, is referred to as an electronic Hamiltonian,

$$H_{elec} = -\sum_{i=1}^{N} \frac{1}{2} \nabla_i^2 - \sum_{i=1}^{N} \sum_{A=1}^{M} \frac{Z_A}{r_{iA}} + \sum_{i=1}^{N} \sum_{j>i}^{N} \frac{1}{r_{ij}}. \qquad (17)$$

The electron-nuclear attraction term in the electronic Hamiltonian depends on r_A, the nuclear positions. Since the nuclear positions are varied infinitesimally, based on the previous assumption, the Born-Oppenheimer approximation is often referred to as an adiabatic approximation. An adiabatic process is defined as a slowly perturbed system, which in spite of the perturbation remains in the original eigenstate, generating a single potential energy surface. The potential energy surface generated is referred to as an adiabatic surface. See Figure 1.2.

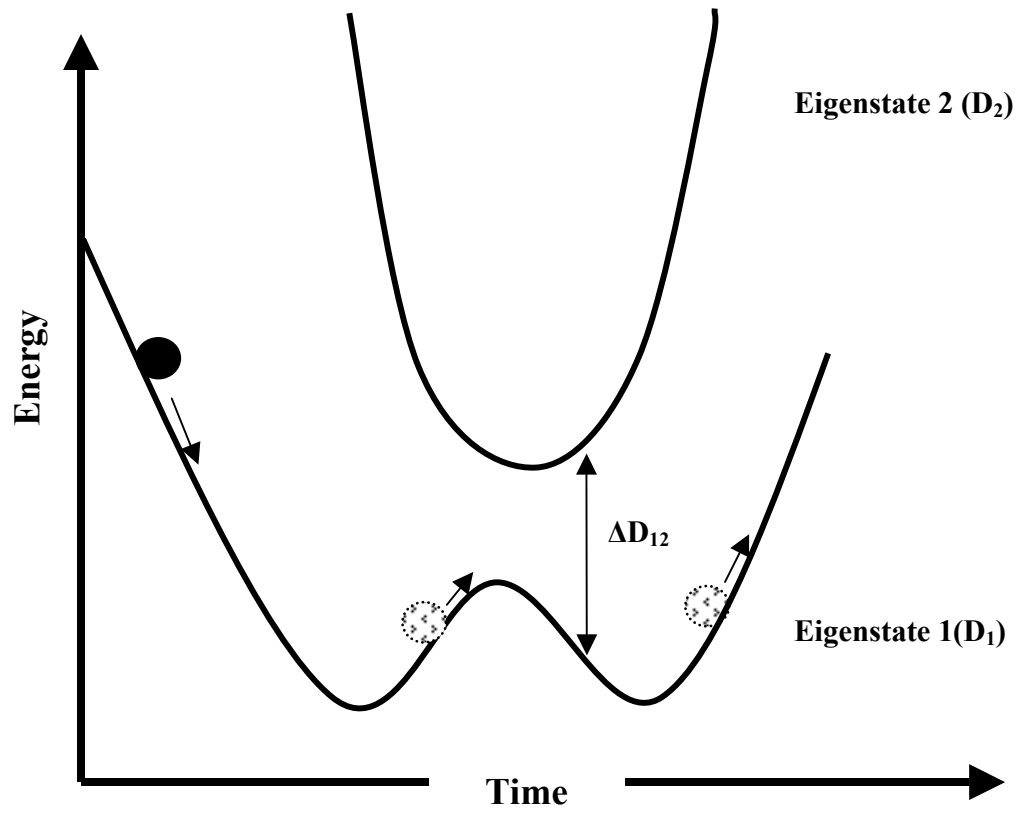

Figure 1.2: Illustration of an adiabatic process. The electron (Black Sphere) moves on eigenstate 1, and remains on eigenstate 1 over a long period of time.

Provided ΔD_{12}, the energy difference between Eigenstate 1 and Eigenstate 2, remains large and the solvent motion is slow, the electron will remain on the ground state, unless the perturbation the electron feels is large enough to induce it to change energy levels. As long as the perturbation is small, the Born-Oppenheimer approximation holds true, but as the perturbation increases the probability of the electron transitioning from one potential energy surface to another increases and the Born-Oppenheimer approximation breaks down.

The Born-Oppenheimer approximation (BOA) also breaks down if two eigenstates of the Hamiltonian are degenerate. Degeneracy of the eigenstates implies two eigenstates have the same energies; therefore the potential energy surfaces corresponding to each of the degenerate eigenstates are indistinguishable. The Born-Oppenheimer approximation is not sufficient to describe these types of systems.

Knowing these limitations exist there have been several attempts to modify the BO approximation. Tuvi *et al*. modified the Born-Oppenheimer approximation by including nonadiabatic coupling correction terms that go beyond the separation of nuclear and electronic interactions. They use a modified Born-Oppenheimer basis (MBOB)[36]that accounts for the interaction between the electronic degrees of freedom and nuclear degrees of freedom.

Esry and Sadeghpour[37], Moss *et al*.[38, 39], and Wolneiwicz *et al*.[40, 41] all studied modifications of the BOA. Each of these studies began with H_2^+, and the addition of a symmetry-breaking term so the BOA can distinguish between isotopically induced HD^+ charge asymmetry. These studies were specifically designed to study electron transfer between two species.

In spite of shortcoming associated with the BOA, our mixed quantum-classical simulation calculations were conducted within the Born-Oppenheimer approximation, and the adiabatic limit. While recognizing that there are several modifications that have improved the BOA, our system of interest is a solvated electron in the ground state. We make no attempts to study transitions of the electron from the ground state to higher energy levels, and have seen no evidence

to support an avoided crossing from the ground state to the first three excited states; therefore the BOA is sufficient to describe our electronic interactions.

1.3 Mixed Quantum-Classical Molecular Dynamics

Unlike CMD, pure quantum mechanical simulations of large systems with thousands of atoms[42] is not currently feasible, due to the limitation of modern computers. Hybrid methods such as mixed quantum-classical molecular dynamics (MQCMD) serve as a bridge between simulating quantum mechanical and classical systems. The use of mixed quantum-classical systems is the gateway to better understanding quantum mechanical processes, in condensed phase systems.

In MQCMD a few critical degrees of freedom are treated quantum mechanically and the solvent molecules are treated classically. The most challenging aspect of employing the use of MQCMD is that the quantum mechanical degrees of freedom must progress accurately, and the classical degrees of freedom must respond correctly to the electronic transitions.

To study the electron using MQCMD systems, a determination whether to include electronic transitions must be made. If electronic transitions are excluded, the Born-Oppenheimer approximation is employed and the electron remains on a single potential energy surface. If electronic transitions are included the simulation becomes nonadiabatic, and the electronic transitions are no longer confined to one potential energy surface.

There are several approaches to describing the interactions of quantum mechanical degrees of freedom with the classical bath. The two most common approaches are the mean-field [43] and the surface hopping[44] methods.

In the mean-field method, the total wavefunction is separated into a product of slow and fast particles. The fast particles correspond to the quantum mechanical particles, and the slow particles correspond to the classical atoms in the system. The classical atoms and electrons in the mean-field approach evolve on a single potential energy surface that is an average of all possible quantum states. Hence in the mean-field approach correlation between electronic states are ignored.

In order to correctly describe the interactions between classical and quantum mechanical dynamics, each quantum state must evolve on a distinct potential energy path. The surface hopping formalism addresses this shortcoming, and each quantum state evolves on a distinct potential energy surface.

In mixed quantum-classical molecular dynamics, the standard molecular dynamics simulation cycle is employed but a significant modification is made. After specifying the initial positions and velocities, the time-independent formulation of Schrödinger's differential equation is solved and new forces, $F_i(t)$, are generated. In CMD, these forces are purely solvent-solvent interactions, but in MQCMD, forces include not only the solvent-solvent interactions, but also the electron-solvent interactions.

Using the new $F_i(t)$, accelerations are calculated and used to propagate velocities and positions. With the exceptions of having used Schrödinger's equation to determine the electron solvent forces, the CMD cycle in both cases remains the same. Refer to Figure 1.3.

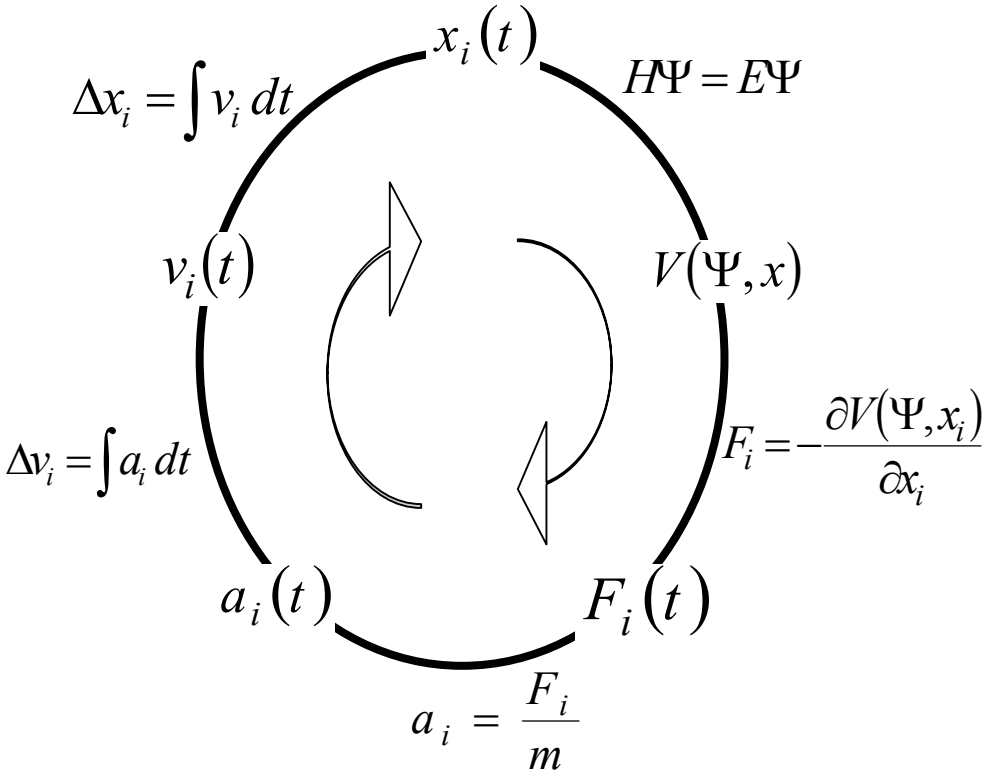

Figure 1.3: Flowchart of events that occur during a mixed quantum-classical molecular dynamics simulation. Positions are represented by $x_i(t)$, $v_i(t)$ represents the velocities and $a_i(t)$ represents the accelerations. The forces are represented by $F_i(t)$, and the potential is represented by $V(\Psi, x)$.

1.4 Hydrated Electrons

When an electron is solvated by water molecules, a hydrated electron is generated. Hydrated electrons play a significant role in electron transfer, condensed phase radiolysis, radical chemistry and photosynthesis. The energetics

(*i.e*. energy levels) of the hydrated electron energy are very sensitive to solvent fluctuations; therefore the hydrated electron serves as a sensitive spectroscopic probe for measuring solvent fluctuations. Hydrated electrons have been used as an experimental tool to study the dynamics of polar liquids[45, 46] and the fluctuations associated with solvation of charged particles[47, 48].

Hydrated electrons have been studied theoretically using mixed quantum classical molecular dynamics[49-53]. Experimental studies of hydrated electrons have also been conducted using both the unpolarized and polarized transient hole burning techniques[54-58], photon echo experiments[59], and resonance Raman spectroscopy[60-62].

Mixed quantum-classical molecular dynamics simulation studies conclude that a hydrated electron can be found in elliptical cavities defined by as few as six water molecules, and energy levels are distributed like the energy levels of a hydrogen atom. In the ground state a hydrated electron exist in a spherical *s*-like cavity, and in the excited state it displays *p*-like characteristics[53, 57, 63-65].

In order to theoretically study hydrated electrons using MQCMD, potentials are needed to calculate the electron-water forces. A potential known as the water-electron pseudopotential, constructed from solid state physics and scattering theories, is used to describe the interaction between the solvent molecules, and the electron[66]. The details of the water electron pseudopotential used in our investigations, will be discussed in detail in Section 3.2.

1.5 Water Models

Computer water models have been developed to help elucidate physical and chemical properties of liquid or supercritical water. Water, a ubiquitous solvent, is vital to human existence. It is a unique solvent because of hydrogen bonding. The hydrogen bonding network in water is responsible for its high surface tension, high specific heat, high boiling and melting points. The quest for a better understanding of water and how it behaves stems from these qualities.

There are several different water models that have been adopted in attempts to simulate liquid water. Among these are the simple point charge (SPC) family of water models: SPC[18], SPC/FLEX[67], SPC/E[18, 68], SPC/HW[69]; the transferable intermolecular potential (TIP) family of water models: TIP3P[70], TIP4P[70], TIP4P-FQ[71], pTIP4P[72-74], TIP3P-Fw[67], TIP5P[75], TIP5P/Ew[76]; and the Stillinger and Weber family of water models: SWFLEX-AI[77], and SWM4-NDP[78].

Generally each water model is parameterized for one or more physical properties of experimental water. Properties such as radial distribution functions, the density anomaly, and critical parameters have all been addressed and correctly predicted by one or more of the currently available water models. Despite the fact that real water has three interaction sites, one oxygen and two hydrogen atoms, theoretical water models differ in geometry, and charge distribution. Most theoretical water models have at least three atomic sites, but they can have as many as five interaction sites or even more. See Figure 1.4.

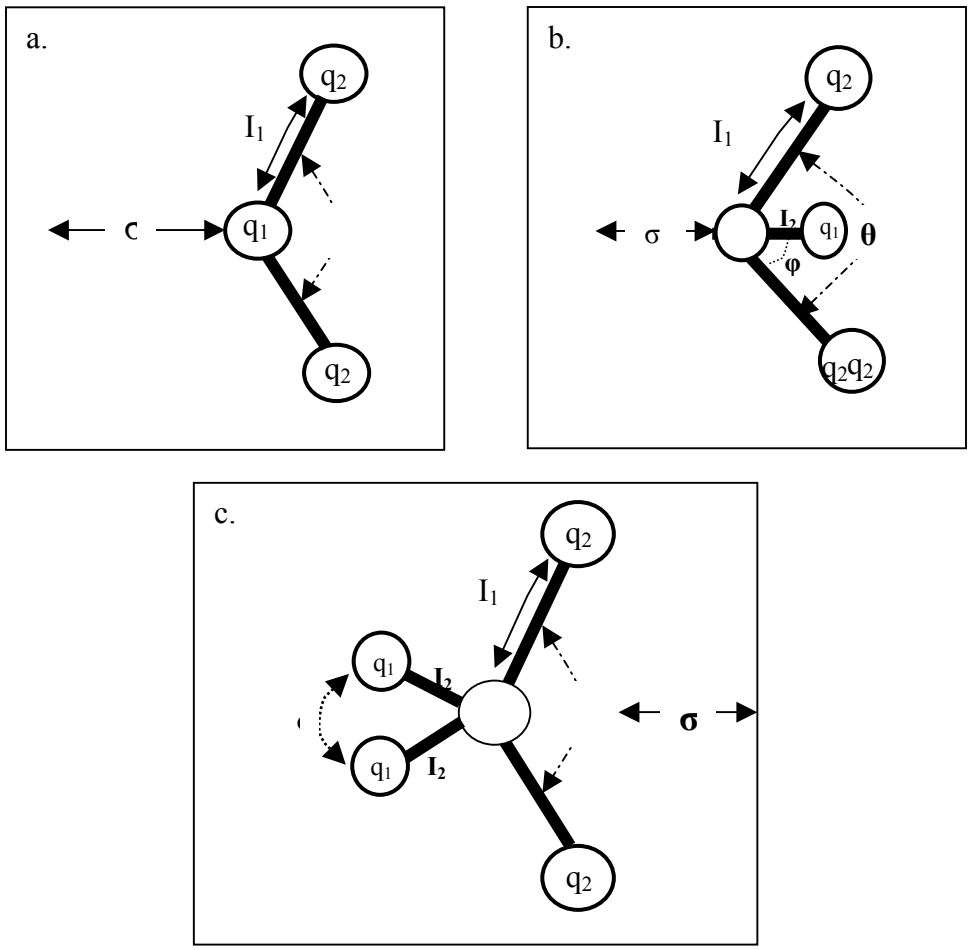

Figure 1.4: Three different geometries of existing water models (Adapted from ref. [79]). All three figures (a-c) represent different types of theoretical water geometries. All of these structures are planar except for 1.4c which has a tetrahedral geometry. Bond lengths are represented by I_1 and I_2, q_1 and q_2 represent charged sites, σ represent the C_2 axis of symmetry, and θ describes the HOH angle. Bond angles, bond lengths, and charges vary from model to model. See Table 1.2.

Bonds within theoretical water molecules can be rigid or flexible. When the bonds are flexible, vibrational properties of experimental water are included in the parameterization of flexible water models, and when they are rigid, the bond lengths are fixed throughout the simulation. Flexible models are denoted by

abbreviations such as FLEX and Fw. Real molecules vibrate; therefore including these properties appears to be the correct approach to better representing experimental water. However, it has been found that including vibration considerations during parameterization increases computational burden and cost, and the improvements, with the exception of self diffusion coefficient, is negligible[80].

Model	Type	l_1 Å	l_2 Å	q_2 (e)	q_1 (e)	θ°	φ°
SPC[18]	a	1	-	0.41	-0.82	109.47	-
SPC/E[68]	a	1	-	0.4238	-0.847	109.47	-
SPC/HW[69]	a	1	-	0.435	-0.87	109.47	-
SPC/Fw[67]	a	1.012	-	0.41	-0.82	113.24	-
TIP3P[70, 75]	a	0.9572	-	0.417	-0.834	104.52	-
TIP3P/Fw[67]	a	0.96	-	0.417	-0.834	104.5	-
TIP4P[70]	b	0.9572	0.15	0.52	-1.04	104.52	52.26
TIP4P-Ew[81]	b	0.9572	0.125	0.52422	-1.048	104.52	52.26
TIP4P-FQ[71]	b	0.9572	0.15	0.631	-1.261	104.52	52.26
TIP4P/Ice[82]	b	0.9572	0.1577	0.5897	-1.179	104.52	52.26
TIP4P/2005[83]	b	0.9572	0.1546	0.5564	-1.113	104.52	52.26
SWFLEX-AI[77]	b	0.9681	0.14[1,3]	0.6213	-1.246	102.71	51.35
SWM4-NDP[78]	b	0.9572	0.24034	0.55733	-1.115	104.52	52.26
ST2 [84]	c	1	0.8	0.24357	-0.244	109.47	109.47
TIP5P[70, 75]	c	0.9572	0.7	0.241	-0.241	104.52	109.47
TIP5P-Ew[76]	c	0.9572	0.7	0.241	-0.241	104.52	109.47

Table 1.2: Geometric parameters for various water models. Bond lengths are represented by I_1 and I_2; q_1 and q_2 represent the charges on atoms or fictitious mass-less sites; and θ, is the HOH angle. Type refers to the type of water model as depicted in Figure 1.4. The angle φ, in Figure 1.4 b, describes the *HOM* angle, whereas in Figure 1.4 c it describes the q_1Oq_2 bond angle.

Water models differ in their approach to evaluating charge distribution on the interaction sites, within each water molecule. For instance, the oxygen on a

TIP3P water molecule carries a negative charge, whereas the oxygen in a TIP4P water molecule has no charge associated with it. In TIP4P water, a negatively charged fictitious site, known as the M-site exists on the bisector of the HOH angle.

Charges can be fixed, or polarizable. If charges are polarizable, the electron or charge density or fluctuating dipole moment is allowed to change based on the local surroundings of each water molecule. Polarizable water models therefore make for a better water model than fixed charge models, in principle. Improving non-polarizable models by adding polarization increases the computational cost, and burden. Despite an increase in the computational burden, polarizable water models have shown a significant improvement in both gas phase and liquid state properties of bulk water; therefore using polarizable water models should generate more accurate results.

Unfortunately there is no single water model that correctly predicts all properties of water.

CHAPTER TWO
STUDY OF TEMPERATURE CONTROL ALGORITHMS

2.1 Introduction

Classical molecular dynamics (MD) simulations are most straightforward to conduct in the microcanonical ensemble, as the equations of motion conserve energy in the limit of small time-steps. Frequently, however, it is desirable to perform simulations in the canonical ensemble, either to model an experimental system in contact with a heat bath, or to allow broader sampling of phase space than is performed when the system is restricted to a single isoenergetic trajectory, or even to mask energy conservation errors and allow a more aggressive timestep to be used. A very common use of a thermostat is to bring the system into equilibrium at a particular temperature, at which point a microcanonical simulation can be performed. In order to perform an MD simulation in the canonical ensemble, a temperature control algorithm, or thermostat, is needed.

There is a great variety of thermostat algorithms that have been employed for the purpose of controlling the temperature. Among these are the Andersen[17], Berendsen[18], Hoover[85], Nosé-Hoover[85-87], Langevin[1], and velocity-rescaling thermostats. These thermostats have all been widely used, but there are very few studies that have directly examined the effects of the thermostat algorithm on the properties of the system, and fewer still that compare multiple thermostats directly. Indeed, it is generally assumed that any thermostat (certainly the one in use in each particular study) is adequate for bringing the system into equilibrium at the desired temperature. It is frequently assumed implicitly (and often

incorrectly) that the thermostat in question will correctly generate an equilibrium system in the canonical ensemble. The purpose of this paper is to illustrate that not all thermostats will even bring a system to thermal equilibrium.

These effects have been observed before, for the velocity rescaling thermostat. In an important study, Harvey *et al.* observed a side effect of the widely used velocity rescaling thermostat that they termed the "flying ice cube" effect.[88] Use of the velocity rescaling thermostat causes the internal motions of the system to become damped towards low energy, while the overall average kinetic energy is maintained through an elevated translational kinetic energy. Thus, prolonged use of the velocity rescaling thermostat, rather than relaxing to thermal equilibrium between the various degrees of freedom, actually leads to sustained violations of energy equipartition.

In a direct comparison of several different temperature control algorithms, Nilsson et al.[89] studied the effect of four thermostats (Hoover, Velocity rescaling, Nosé-Hoover and Berendsen) on the physical properties of 7208 SPC/E[90] and TIP3P[70] water molecules. In their analysis of energetic, structural, and dynamic properties they reported that the flying ice cube effect was not observed in their simulations. However, they did report the existence of unexplained problems when using deterministic thermostats such as the velocity rescaling thermostat. Among the observed problems are a pronounced departure from linearity in the mean square displacement plots, and an inability of the thermostat to maintain the systems temperature at the target temperature.

In this study we apply four commonly used thermostats in the simulation of bulk TIP4P water. The four thermostats chosen are the velocity rescaling, Andersen, Langevin, and Berendsen thermostats. The primary emphasis is on the partitioning of system energy between the rotational and translational degrees of freedom, and how this differs for different thermostats. The effects of any violations of equipartition on the dynamic behavior of liquid water are also considered.

Our primary observation is that the flying ice cube effect is not limited to the velocity rescaling thermostat. This phenomenon also occurs in the Berendsen thermostat, and should be expected to occur in any thermostat that performs a deterministic, rather than stochastic, perturbation of atomic velocities in a way that depends on the system temperature. Echoing and extending the results of Harvey et al., we find that over long periods of time, deterministic thermostats do not partition the energy of the system correctly, and lead instead to a steady state that is not only non-canonical, but is not in thermal equilibrium. On the other hand, we confirm that stochastic thermostats such as the Andersen and Langevin algorithms correctly bring the rotational and translational subsystems into thermal equilibrium, as should occur for proper equilibration in the canonical ensembles.

The computational details and specific thermostat algorithms are discussed in Section II. The simulation results are presented in Section III, and in section IV we summarize the results and their significance for those performing thermostatted molecular dynamics simulations.

2.2 Computational Details

Simulations of TIP4P water were performed in both the bulk liquid phase and as a gas-phase dimer, using each of four thermostats: velocity rescaling, Andersen[17], Berendsen[18], and Langevin[1]. In the bulk water simulations, 200 TIP4P water molecules were used in a cubic box, of length of 18.17 Å, resulting in a density of 0.9974 g/cm^3. Periodic boundary conditions were employed, with the minimum image convention. In each simulation, an equilibration period of 1.5 ns (dimer) or 2 ns (bulk) was followed by a period of 1 ns during which results were collected. The velocity Verlet algorithm[91, 92] was used to integrate the equations of motion with a timestep of 1 fs, and the RATTLE algorithm[93] was used to constrain the rigid bonds in TIP4P water.

The system temperature was calculated from the kinetic energy in the usual way, using the assumption of equipartition of energy. A system with N particles and N_c constraints will have $3N–N_c$ degrees of freedom. If each is assumed to have a kinetic energy of $kT/2$, the full system temperature can be calculated from the total kinetic energy as

$$T_{tot} = \frac{2KE}{(3N - N_c)k} = \frac{1}{(3N - N_c)k} \sum_{i=1}^{N} m_i v_i^2 . \qquad (1)$$

In a system of 200 TIP4P water molecules, for example, there are N=800 particles (including the M sites) and N_c=1203 constraints, including six bond length constraints per water molecule, plus three constraints on the conserved center-of-mass translational velocity). Thus there are $3N–N_c$=1197 degrees of freedom for this system (three linear and three angular velocities per water

molecule, less the three constraints on the system's center-of-mass linear velocity).

In order to evaluate the extent to which equipartitioning is obeyed, the total system temperature will be decomposed into rotational and translational temperatures. The translational temperature, T_{tr}, is calculated using only the kinetic energy due to center-of-mass translations,

$$T_{tr} = \frac{2KE_{tr}}{(3N_{mol} - 3)k} = \frac{1}{(3N_{mol} - 3)k} \sum_{i=1}^{N_{mol}} M_i \left(v_i^{com}\right)^2, \tag{2}$$

where M_i is the mass and v_i^{com} is the center-of-mass velocity of molecule i, and there are a total of N_{mol} molecules. Only the three constraints on the system's center-of-mass linear momentum are attributable to the translational subsystem.

For a system of rigid TIP4P molecules, there is no vibrational kinetic energy (all $6N_{mol}$ vibrational degrees of freedom are constrained), and all non-translational contributions to the kinetic energy are rotational. Consequently the rotational temperature is calculated from the rotational kinetic energy as

$$T_{rot} = \frac{2KE_{rot}}{3N_{mol}k} = \frac{1}{3N_{mol}k} \left[\sum_{i=1}^{N} m_i v_i^2 - \sum_{i=1}^{N_{mol}} M_i \left(v_i^{com}\right)^2 \right], \tag{3}$$

here there are three rotational degrees of freedom per molecule. (The rotational angular momentum of the full system is not constrained, due to the periodic boundary conditions.)

Next, the algorithms used to implement each of the four thermostats are described in Chapter 1, along with some of their important features. The specific temperatures and details pertaining to the simulation details using each of the four thermostats, is described below.

Using the velocity rescaling thermostat, we scale the velocities whenever the instantaneous system temperature exceeds the range $[T_0 - \Delta T, T_0 + \Delta T]$, where T_0 is the reference temperature (chosen to 298.15 K here, in all simulations) and ΔT is a tolerance used to specify the strictness of the temperature control (chosen to be ΔT = 3 K).

The velocity reassignments for the Andersen thermostat occur for all atoms simultaneously, and these global collisions with the heat bath occur once every 100 fs.

The friction coefficient for the Langevin thermostat was selected arbitrarily and at every timestep the random force is selected from a Gaussian distribution.

The Berendsen thermostat, like the velocity rescaling thermostat scales the velocities, but here the scaling is performed at every timestep. The reference temperature for the Berendsen thermostat is 298.15 K.

2.3 Results / Discussion

The primary goal of this study was to investigate the extent of any violations of equipartitioning of energy induced by each of the four thermostats investigated. For the rigid TIP4P water model, there are no vibrational degrees of freedom. Consequently, the main results examined are the rotational temperature, T_{rot}, and the translational temperature, T_{tr}.

Both the Berendsen and velocity rescaling thermostats fail at maintaining the correct energy distribution between the various degrees of freedom in the

simulated water systems. We observed both deterministic thermostats exhibit the flying ice cube effect. The flying ice cube effect, reported as an inherent problem associated with rescaling thermostats, is a result of a continuous increase in the ratio of the reference and instantaneous temperatures, due to thermal fluctuations. Due to the aforementioned problems in an isolated MD system where rescaling thermostats are used, as the energies associated with translational degrees of freedom increase, the internal energies such as rotations or vibrations become extremely small[88].

In our simulation studies we compared the energies and temperatures of four thermostats and as expected the stochastic thermostat correctly partitioned the energies of all degrees of freedom. The deterministic thermostats on the other hand partitioned the energies of the various degrees of freedom incorrectly but maintained the average temperature at the correct value.

In Figure 2.1 a and 2.1 b both systems were equilibrated using the Langevin thermostat, and then a 1 ns simulation period in which the Berendsen thermostat was turned on, and allowed to maintain the temperatures for the length of the simulation. The same procedure was used to obtain Figure 2.1 b, but instead of using the Berendsen thermostat the velocity rescaling thermostat was used. We observed that the Berendsen thermostat is less efficient at maintaining the correct energy distributions for the translational and rotational energies when compared to data obtained using the velocity rescaling thermostat.

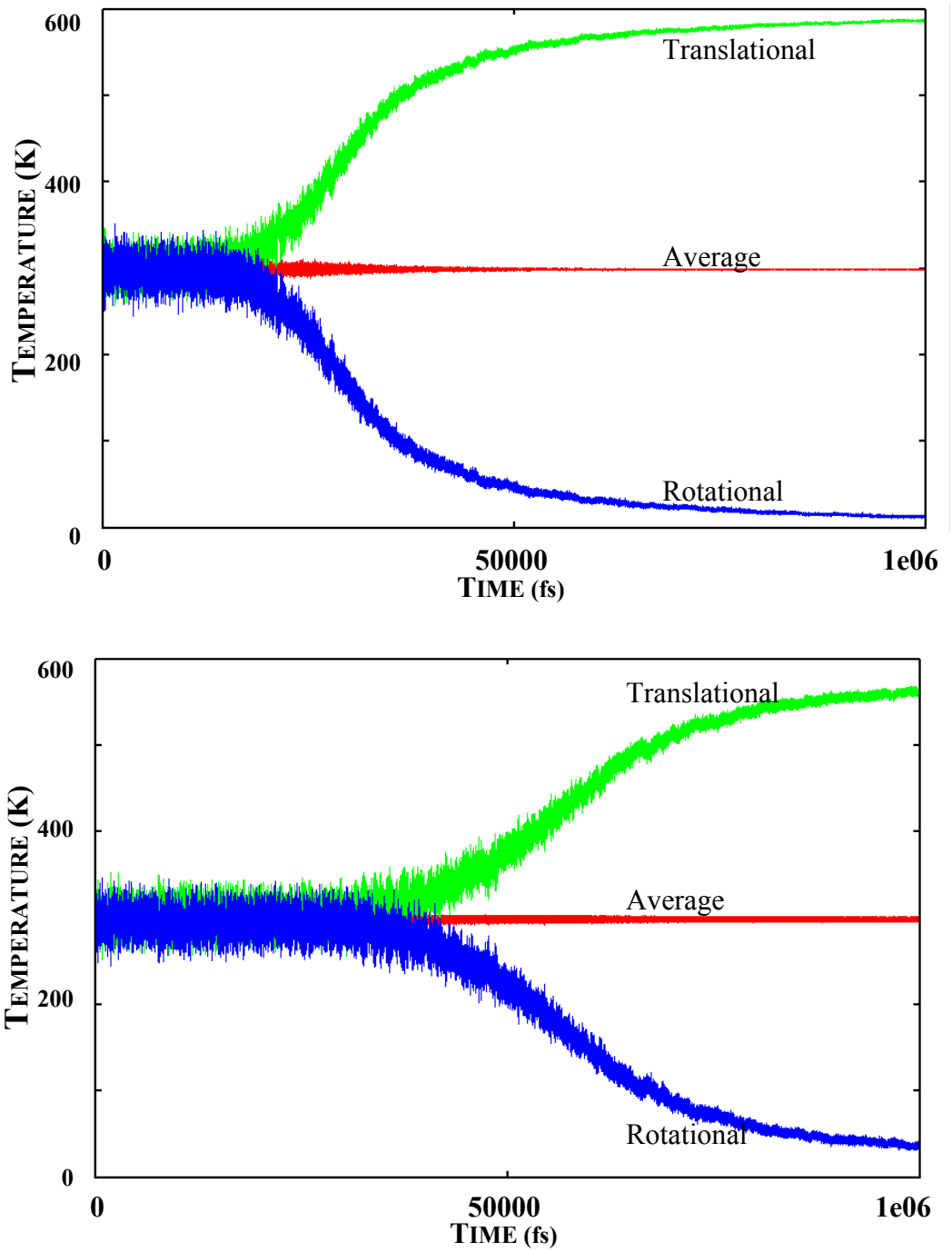

Figure 2.1: Temperature (K) versus time (fs) simulation of TIP4P water molecules. a) Plot generated using the velocity rescaling thermostat b) Plot generated using Berendsen thermostat. Green represents the translational degrees of freedom, red represents the average temperature and blue represents the rotational degrees of freedom.

Using the Berendsen thermostat, after125 ps evidence of partitioning was first observed, whereas in the case velocity rescaling thermostat, partitioning was first observed at approximately 275 ps. After the initial separation in energy occurs, a rapid separation period followed. This rapid separation in energy is substantiated by the magnitude of the derivatives associated with the slopes of the translational and rotational temperatures as seen in Figures 1a and 1b. We also observed that as the system approaches equilibrium, there is a decrease in the rate of energy transfer between the various degrees of freedom.

The flying ice cube effect allows for a continuous transfer of energies from the rotational kinetic energy to the translational kinetic energy, and the magnitude of the rotational kinetic energy continues to approach zero. Therefore it is impossible to attain perfect equilibrium. The values we utilize in tables 1 and 2 are specific to the length of our simulations.

Thermostats	**Langevin**	**Velocity Rescaling**	**Andersen**	**Berendsen**
T_{ref}	298.15 K	298.15 K	298.15 K	298.15 K
T_{avg}	300 ± 1 K	299.06 ± 0.03 K	297 ± 1 K	298.476 ± 0.004 K
T_{rot}	299 ± 2 K	12.9 ± 0.2 K	296 ± 2 K	9.2 ± 0.1 K
T_{trans}	302 ± 2 K	871.3 ± 0.4 K	300 ± 3 K	877.1 ± 0.2 K
T_{trans} / T_{rot}	1.01 ± 0.01	67.54 ± 0.02	1.013 ± 0.01	95.33 ± 0.01

Table 2.1: Calculated temperature and standard deviation values for the water dimer simulations for each of the four thermostats used in our simulations.

Thermostats	Langevin (K)	Velocity Rescaling (K)	Andersen (K)	Berendsen (K)
T_{ref}	298.15	298.15	298.15	298.15
T_{avg}	300.4 ± 0.2	298.14 ± 0.07	298.1 ± 0.2	298.418 ± 0.001
T_{rot}	298.6 ± 0.2	26.0 ± 0.2	296.4 ± 0.2	9.42 ± 0.01
T_{trans}	302.3 ± 0.2	571.7 ± 0.2	299.9 ± 0.2	596.60 ± 0.01
T_{trans} / T_{rot}	1.012 ± 0.001	21.988 ± 0.008	1.013 ± 0.001	63.33 ± 0.001

Table 2.2: Calculated temperature and standard deviation values for the bulk water simulations for each of the four thermostats used in our simulations. Temperatures T_{ref}, T_{rot}, T_{trans} are in units of Kelvins, but T_{trans} / T_{rot} is unit less.

The ratios of translational temperature and rotational temperatures, T_{trans} / T_{rot}, have been calculated for bulk and dimer simulations. These values are reported in tables 1 and 2. For the Andersen and Langevin thermostats the ratios of T_{trans} / T_{rot} are approximately one, whereas the rescaling thermostats deviated by a great deal from unity. In the bulk systems, the velocity rescaling thermostat had a T_{trans} / T_{rot} ratio of 63.33 ± 0.001, and the Berendsen thermostat had a ratio of 21.988 ± 0.001.

The consequence of equipartion violation is very severe and distorts the dynamics of atoms for extensively long periods even after the deterministic thermostats were turned off. We turned off the Berendsen thermostat after the 1 ns data acquisition period, and attempted to calculate how long it takes for the energies of the translational and rotation kinetic energies to return to an average

of 298.15 K. Two successive simulations were performed, both were 1 ns long. Our focus was on the rotational energies and we calculated the extent of heat absorbed by the internal energies. The results were surprising, and they are as follows. After the first 1 ns second run, the average rotational temperature was 22.419 ± 0.004 K, and after the second 1 ns run the average rotational temperature was 21.955 ± 0.005 K. After 2 ns the bulk water system had heated up by 0.4671 ± 0.0003 K. This simulation is characteristic of several simulations performed under the same conditions. As we mentioned earlier, these values we report are representative of the duration of the simulation length, but the pattern of energy distribution is consistent among all our simulations.

Harvey et al. in their 1997 study of temperature control algorithms on SPC/E water observed that there is a dependency on the system size and the extent of energy separation among different degrees of freedom in the system. We explored this observation and extended our studies beyond observations of bulk water simulations. We studied water dimer(s) using each of our four thermostats and compared the obtained temperature values to the temperatures obtained in bulk water simulation. In the dimer simulations, we observe that the extent of equipartition violation is larger than in the bulk water simulations. See tables 1 and 2.

The translational temperatures associated with the Berendsen thermostat for the water dimer is 877.1 ± 0.2 K, whereas the bulk water has a translational temperature of 588.9 ± 0.4 K. The magnitude of the difference we observe between bulk and dimer translational temperature is also evident when the

velocity rescaling thermostat is used. There is a significant increase in the translational temperature as the system size decreases and the flying ice cube effect is much more pronounced.

Self diffusion coefficient values for TIP4P water were calculated after equilibration in a non-thermostatted environment using Einstein's equation,

$$D = \lim_{t \to \infty} \left[\frac{\left\langle |r(t) - r(o)|^2 \right\rangle}{6t} \right], \tag{4}$$

where r represents the position of the atoms at any given time. The non-thermostatted simulations were performed for 1ns. From our simulations we observed that both stochastic thermostats did not distort the dynamics of the water molecules. The microcanonical simulations we ran after employing the use of both the Andersen and Langevin thermostats generated self diffusion coefficient values that are in good agreement with literature values for the TIP4P water model. Refer to Table 3.

Thermostats	Type	Diffusion Coefficients (cm^2/s)
Berendsen	Deterministic	5.56×10^{-5}
Andersen	Stochastic	3.44×10^{-5}
Langevin	Stochastic	3.78×10^{-5}
Velocity Rescaling	Deterministic	5.44×10^{-5}
Theoretical TIP4P	None	$3.6\ (0.2) \times 10^{-5}$ [71]
Experimental	-	2.4×10^{-5} [94]

Table 2.3: Theoretically calculated self diffusion coefficient values calculated after applying each of the four thermostats.

The deterministic thermostats on the other hand, overestimated the mean squared displacement values and this is most likely a result of the violation of energy equipartition. At the end of the equilibration period, the translational degrees of freedom in both the Berendsen and velocity rescaling thermostats increased a great deal, and average values of 596.60 ± 0.01 K, and 571.7 ± 0.2 K, respectively, were reported. It is logical to assume that molecules will diffuse faster as the translational temperatures increase, and in fact we observe this phenomenon and report values of all diffusion coefficient values in Table 3.

We recommend that for each simulation the choice of thermostat should depend on the experiment and data been collected. Keeping in mind that as translational energy increases and rotational energy decreases the physical meaning of the system of study begins to break down.

2.4 Conclusion

The use of deterministic thermostats such the Berendsen and velocity rescaling thermostats have inherent problems associated with them. Without modifications such as periodically removing center of mass motions, and performing infrequent rescaling, these thermostats will severally dampen the internal energies, and extremely increase the linear momentums of atoms in the system. In this paper we make no attempt to discuss possible methods for improving the rescaling methods. Our goal is to illustrate the extent to which these thermostats differ from stochastic thermostat and partition energies with regards to the various degrees of freedom in the system. Also comparing self diffusion coefficient values obtained from each thermostat go to further illustrate how each thermostats change the dynamics of system. We find that to calculate self diffusion for water it is ill advised to employ the use of deterministic thermostats, such as the Berendsen and velocity rescaling thermostats, because energy equipartition is violated, and this leads to severe distortion of dynamical properties such as diffusion statistics.

CHAPTER THREE
MIXED QUANTUM-CLASSICAL STUDY OF A HYDRATED ELECTRON: I. EFFECTS OF WATER GEOMETRY

3.1 Introduction

Hydrated electrons play a significant role in condensed phase radiolysis, radical chemistry, and photosynthesis. To better understand electron transfer in these processes, extensive theoretical studies have been conducted on the behavior, properties and dynamics of a single electron in water. A variety of water models have been used to study hydrated electrons in the past, ranging from rigid, nonpolarizable models (SPC)[18] to flexible models (SPC/Flex)[67] and polarizable models (pTIP4P)[72-74]. Rossky et al.,[50, 51, 95, 96] have studied the adiabatic and nonadiabatic dynamics of an electron in SPC/Flex water. Staib and Borgis examined the shape fluctuation and diffusion of an electron using the floating spherical Gaussian orbital (FSGO) method[97] using a polarizable version of TIP4P water (pTIP4P) [72-74].

The computed ground state absorption spectrum is one of the key quantities discussed in these studies, and is repeatedly found to be blue shifted by 0.5–0.7 eV from the experimental absorption peak. A new electron–water pseudopotential was developed by Turi and Borgis[66] and used to model the hydrated electron in SPC water. This new pseudopotential addressed the blue shift in the computed absorption spectrum; the average energy difference between the ground and first excited state of 1.7 eV in this study[66], was much lower than the value of 2.2 eV that had been previously calculated[50,95,57, 66, 98-100]. The shape of

the simulated absorption spectrum was well reproduced, however, with absorption overestimated at low energies and underestimated in the high-energy tail.

Del Buono *et al*. studied the diffusive transport of a hydrated electron in SPC-FLEX water[49]. They compared the diffusive behavior of the hydrated electron to that of a hydrated bromide ion in SPC water in order to elucidate the factors responsible for the enhanced diffusion rate of the hydrated electron in comparison to the halide ions[49].

Despite the variety of models used to study the hydrated electron, no attempt has been made to quantitatively assess the effect of different water models, or their different features, on the properties of the simulated wet electron. In this study, we explore the structural, energetic, and dynamical properties of a hydrated electron solvated by two different water models. Here, we focus on the simple point-charge (SPC) model and the four-point transferable intermolecular potential (TIP4P). These models were chosen both for their popularity and their simplicity. Both are rigid, nonpolarizable models. While it is easily argued that a flexible or polarizable model should provide better comparison with experiment, the goal in using these two models is to isolate the effect of the geometry of the water model. The effects of flexibility and polarizability are mentioned briefly below, but a detailed analysis of these features is not considered here.

The SPC and TIP4P water models differ in their underlying geometries, as well as in their computed thermodynamic properties. The SPC water model has three interaction sites, located on the atomic nuclei, whereas the TIP4P water has four interaction sites: the three nuclei and a massless site known as the M site,

which is on the bisector of the HOH angle, shifted inward from the oxygen site towards the center of mass. The site of negative charge in the SPC model is on the oxygen, while in the TIP4P model it resides on the M site. The parameters defining both water models are listed in Table 3.1.

Potential Parameters	SPC	TIP4P
r_{OH} (Å)	1.00	0.9572
r_{OM} (Å)	—	0.15
θ_{HOH} (deg.)	109.47	104.52
ε (kcal/mol)	0.1554	0.1550
σ (Å)	3.166	3.154
q_H(e)	+0.41	+0.52
q_M(e)	—	–1.04
q_O(e)	–0.82	0.00

Table 3.1: Potential geometric parameters for SPC and TIP4P water models[18, 70].

Calculated properties for the two water models are listed in Table 3.2, along with experimental values. The TIP4P potential is typically considered to be a more accurate model of liquid water, because several properties of bulk water (such as the heat capacity and enthalpy of vaporization) and the water dimer (bond energy and angle) are better represented by TIP4P than SPC. The TIP4P model also gives a more accurate representation of the structure of liquid water[70].

Property	SPC	TIP4P	Experiment
Gas phase dipole moment, μ (D)	2.27[a]	2.18[a]	1.85[b]
Dimer Energy (kcal/mol)	–6.59[a]	–6.24[a]	–5.44 (0.7)[c]
Dimer O-O Length (Å)	2.75[a]	2.75[a]	2.98[d]
Water dimer angle (deg)	21° [a]	46° [a]	60° [d]
C_P (cal mol^{-1} deg^{-1})	23.4 [a]	19.3 [a]	17.99 [d]
ΔH_{vap} (kcal/mol)	10.77 [a]	10.66 [a]	10.51 [d]
ρ (g/cm^3)	0.971 [a]	0.999 [a]	0.997 [d]
Diffusion constant (10^{-5} cm^2/s)	3.3[e]	3.6[e]	2.4[f]

Table 3.2: Calculated properties for SPC and TIP4P water potentials, and experimental properties of water.

The goal of this work is to perform simulations of the energetics and dynamics of the hydrated electron that differ only in the treatment of the solvent, in order to determine how much role the water model plays in governing the behavior of the hydrated electron. In section II, we discuss the details of our simulations, and the pseudopotential used for the electron-water interaction. In section III, we present and discuss the properties of the hydrated electron when solvated by both water models. Conclusions are presented in section IV.

3.2 Simulation Details

A. Potential Details

The water-electron interactions are described in these simulations via the Rossky and Schnitker electron-water pseudopotential[51]. While the newer Turi and Borgis pseudopotential provides absorption energies that are in better agreement with experiment, the goal here is to study the effect of the water model, rather than the pseudopotential. Because more simulations have been performed with the Rossky and Schnitker pseudopotential, we use that model here to facilitate comparison with previous work.

The electron–water pseudopotential can be written as

$$V_{ps}(\mathbf{r}) = \sum_i S(|\mathbf{r}-\mathbf{r}_i|)\frac{-q_i}{|\mathbf{r}-\mathbf{r}_i|} - \sum_{\mathrm{O}}\left[1-e^{-(|\mathbf{r}-\mathbf{r}_\mathrm{O}|/r_C)^6}\right]\frac{\alpha_0}{2|\mathbf{r}-\mathbf{r}_\mathrm{O}|^4} + \sum_i\sum_j B_j^{(i)} r^{n_j^{(i)}} e^{-\rho_j^{(i)}|\mathbf{r}-\mathbf{r}_i|}, \quad (1)$$

where the first sum represents the electrostatic interactions, and runs over all interaction sites i with position $\mathbf{r}_i$ and charge q_i. In the TIP4P model the oxygen site is neutral. $S(r)$ is a cubic spline that smoothly turns off the electrostatic interaction inside a cutoff distance r_u, in order to avoid singularities when the electron interacts with a positive nucleus[51]. This cutoff function equals one at distances beyond r_u = 0.4 Å for hydrogen atoms and 0 Å for oxygen (SPC) and the M site (TIP4P). The second term in the pseudopotential represents the polarization potential, resulting from polarization of the water molecule induced by the electron. This term is required because both water models are nonpolarizable, and are parameterized around the effective mean-field polarization induced only by the solvent environment. The molecular polarizability is taken to be α_0 = 9.745 a.u. and is taken to act only at the oxygen

nuclei, for both water models. A cutoff radius of r_C = 1.53 Å prevents the polarization potential from diverging at the oxygen sites. Lastly, the final sum represents the core repulsion potential arising from a double-ζ basis set of Slater orbitals. For both water models, these Slater orbitals are centered on the atomic nuclei, with no orbitals residing on the TIP4P M site. The values of the constants *B*, *n*, and *r* that characterize this effective interaction with the water pseudo-wavefunction can be found in the original description of the pseudopotential[51, 95].

For both the SPC and TIP4P potentials, the water–water interaction potential is a combination of a 12-6 Lennard-Jones potential and electrostatic interactions,

$$U_{\text{int}} = \sum_{i<j} 4\varepsilon\left[\left(\frac{\sigma}{r_{ij}}\right)^{12} - \left(\frac{\sigma}{r_{ij}}\right)^{6}\right] + \sum_{i<j}\left(\frac{q_i q_j}{r_{ij}}\right). \qquad (2)$$

The difference between the two potentials arises in which sites (H atoms, O atoms, or M sites) are LJ or electrostatic interaction sites, and in the values of the ε and σ parameters. The parameters for each model are provided in Table 1.

B. Computational Details

Two mixed quantum-classical systems were studied. The first system contained one electron solvated by 200 SPC water molecules and the second system contained one electron solvated by 200 TIP4P water molecules. Both systems were simulated at constant volume in a cubic box of length 18.17 Å, resulting in a density of 0.997 g/cm^3. Periodic boundary conditions were used, with the minimum image convention[1]. Both systems were equilibrated for 140 ps at a temperature of 298±1 K using the Andersen thermostat[17] with a resampling

interval of 100 fs, and 60 ps of non-thermostatted dynamics followed, during which time all of the property averages were collected. The velocity Verlet algorithm was used to integrate the dynamics with a time-step of 1 fs, and the RATTLE algorithm[93] was used to satisfy the rigid bond constraints in the SPC and TIP4P models.

In the mixed quantum-classical system, the time evolution is treated within the Born-Oppenheimer approximation, with the quantum electron moving adiabatically on the ground state electronic surface. This ground state surface is obtained by solving Schrödinger's equation at every time-step on a spatial grid of 16^3 grid points using an iterative block Lanczos scheme[101]. The solvent evolves under the classical forces due to the gradient of the water–water potential, as well as the quantum (Hellman-Feynman) force[52] due to the electron.

3.3 Results / Discussion

The properties of the hydrated electon are similar in both solvent models, but with some significant differences. The structure (size) of the electron, its energetics, and its mobility are compared below.

The average radius of gyration is used as a measure of the size of the hydrated electon. When the electron is solvated by SPC water, the average (and standard deviation of the) radius of gyration is found to be 2.1(0.2) Å, whereas in TIP4P water the average radius of gyration is 2.0(0.1) Å. This difference is small, but statistically significant. Figure 3.1 shows the distribution of radii of gyration

obtained in both the SPC system and the TIP4P system. The electron is slightly more diffuse in SPC water than in TIP4P.

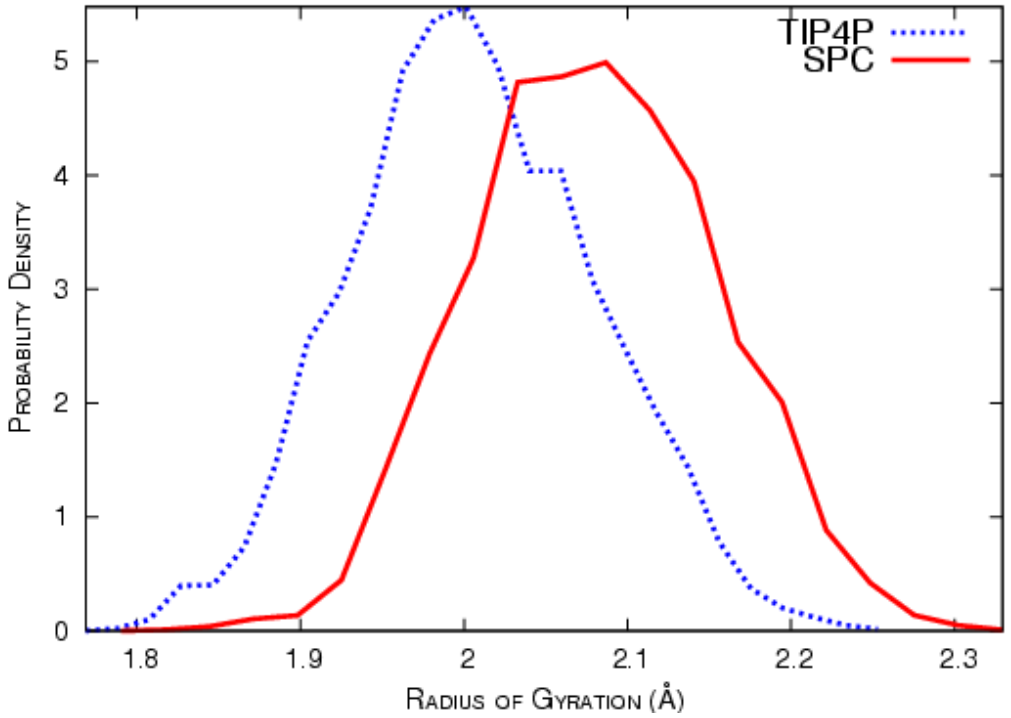

Figure 3.1: Normalized probability density function for the radius of gyration of a hydrated electron solvated by TIP4P water (dashed, blue line) and SPC water (solid, red line).

On the other hand, calculated values of the diffusion coefficient show that the electron is more mobile in TIP4P solvent. Diffusion coefficient values were calculated from 3 ps of a non-thermostatted dynamics, using Einstein's relation,

$$D = \lim_{t\to\infty} \frac{\left\langle |r(t) - r(0)|^2 \right\rangle}{6t} \qquad (3)$$

where r represents the center-of-mass position of the electron. The diffusion constants for the electron in SPC and TIP4P water are 1.55×10^{-5} cm^2/s, and

1.75×10^{-5} cm^2/s, respectively, as calculated from the slope of the mean square displacement with time, at long times. The slightly faster diffusion of the electron in TIP4P water is probably a result both of the slightly smaller size of the electron, as well as the faster dynamics of the TIP4P solvent itself. For the self-diffusion coefficient of water, we obtain a value of 3.94×10^{-5} cm^2/s for TIP4P water, somewhat faster than the diffusion coefficient of 3.38×10^{-5} cm^2/s for SPC, and in agreement with previous results[70]. The calculated diffusion coefficients for the hydrated electron are considerably smaller than those measured experimentally; the experimental diffusion constant calculated for a hydrated electron using the Nernst equation is 4.9×10^{-5} cm^2/s (Ref. [102]). In previous simulations by Rossky and Schnitker using SPC-FLEX water molecules, an electron diffusion coefficient of 3.3×10^{-5} cm^2/s was obtained[96]. The enhanced diffusion they observed is likely due to the type of water model they employed. With a flexible water model, the O–H bond vibration allows the electron greater freedom to move throughout the solvent than in a rigid water system. The solvent self-diffusion coefficient is much more strongly affected by bond length[67] than bond flexibility[79], but the light electron is able to move on the time scale of covalent bond vibration, so flexible bonds have a larger effect.

At equilibrium the ground-state hydrated electron occupies an approximately spherical cavity, while the first three excited states have *p*-like geometry[53, 101]. The energies of these four states are distributed as shown in Figure 3.2. The cumulative distributions are shown in order to most clearly show the energetic shifts due to the solvent model.

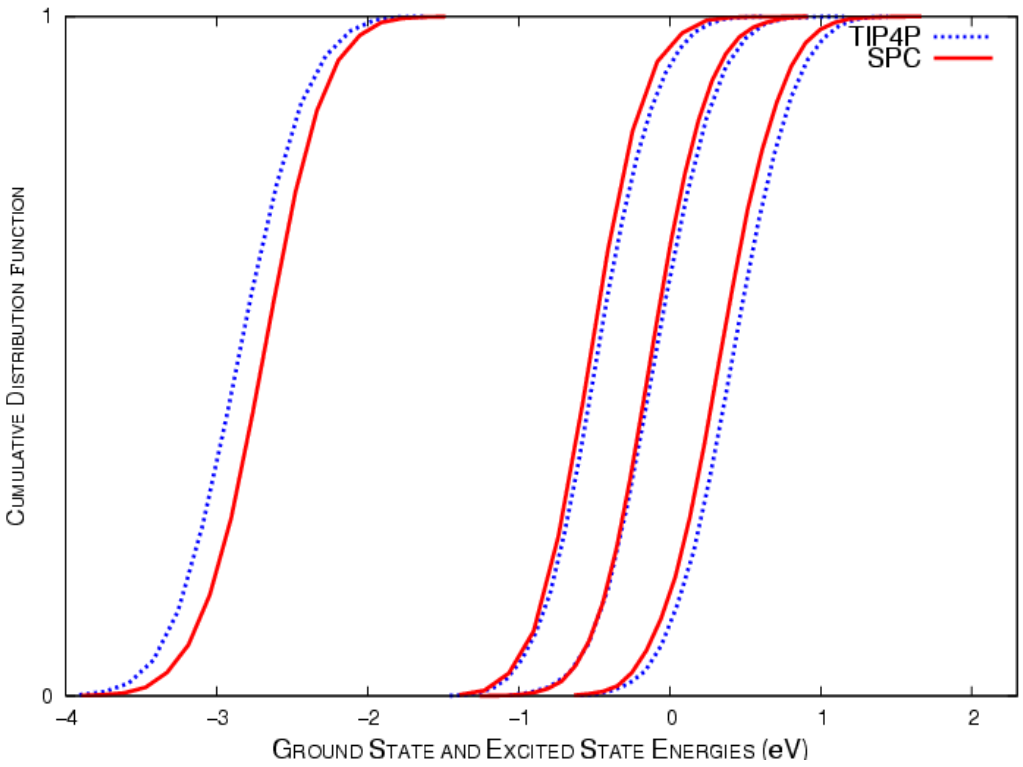

Figure 3.2: Cumulative distribution functions for the energy levels associated with the electron solvated by TIP4P (dashed, blue lines) and SPC (solid, red lines) water).

In TIP4P water, the average eigenenergy of the ground state is -2.79 ± 0.3 eV, somewhat lower than the average ground state energy of -2.59 ± 0.2 eV in SPC water. The experimental value is about 20% lower still, at -3.32 eV (Ref. [100]).

The energy of the *p*-like excited states, on the other hand, are slightly higher in TIP4P water than in SPC water, with a slightly wider splitting of the *p*-like energies. We find a difference of 0.83 eV ± 0.03 between the average energies of the first and third excited state in SPC water, increasing to 0.89 eV ±

0.03 in TIP4P water. The former agrees well with the value of 0.8 eV reported by Schwartz *et al*.[57]

The lowering of the ground state energy and destabilization of the excited states in TIP4P water leads to a simulated absorption spectrum that is blue-shifted when compared to that observed in SPC water, as shown in Figure 3.3.

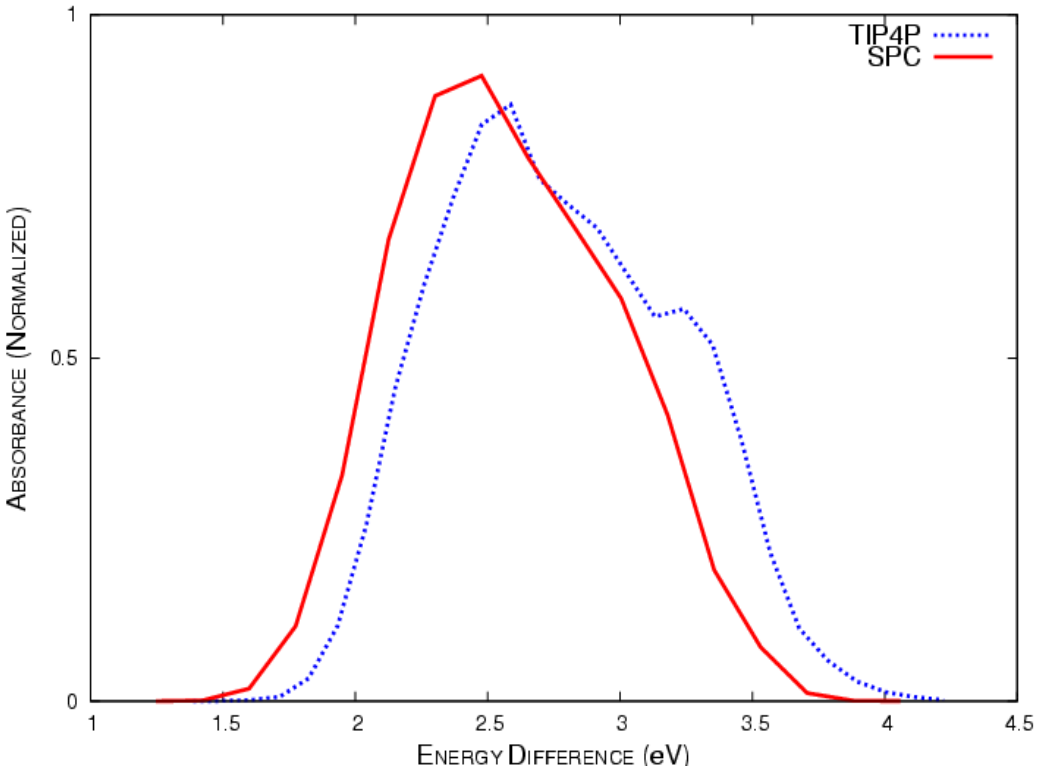

Figure 3.3: Simulated absorption spectra for the hydrated electron in TIP4P (dashed, blue line) SPC (solid, red line) water.

Both spectra are already blue-shifted from the experimental absorption spectrum[103], which has a maximum at 1.7 eV. The experimental spectrum is also both broader and more asymmetric than the simulated absorption spectra, with a full width at half-maximum (FWHM) of 0.84 eV[103]. This blue shift is thus more

pronounced for TIP4P than SPC, which have maxima at 2.6 and 2.5 eV, respectively. The simulated absorption spectrum in TIP4P water is somewhat broader, however, and more asymmetric. The FWHM increases from 1.13 eV in SPC water to 1.28 eV in TIP4P water. The shape of the simulated absorption spectrum is thus slightly better reproduced by TIP4P water, despite the larger blue shift.

The width of the absorption lineshape results in part from the splitting between the three different *p*-like states due to cavity asymmetry, and in part from the broadening of the ground and excited states by solvent fluctuations. If the memory of the cavity asymmetry persists for times longer than a few ps (the lifetime of the excited state), then there is inhomogeneous broadening. Simulations by Schwartz and Rossky in SPC water indicated that the *p*-like states interconverted on time scales of ~1 ps[57, 64], perhaps slow enough to demonstrate inhomogeneous broadening.

In our simulation the splitting patterns observed for both the SPC and TIP4P water-electron simulations are shown in Figure 3.4.

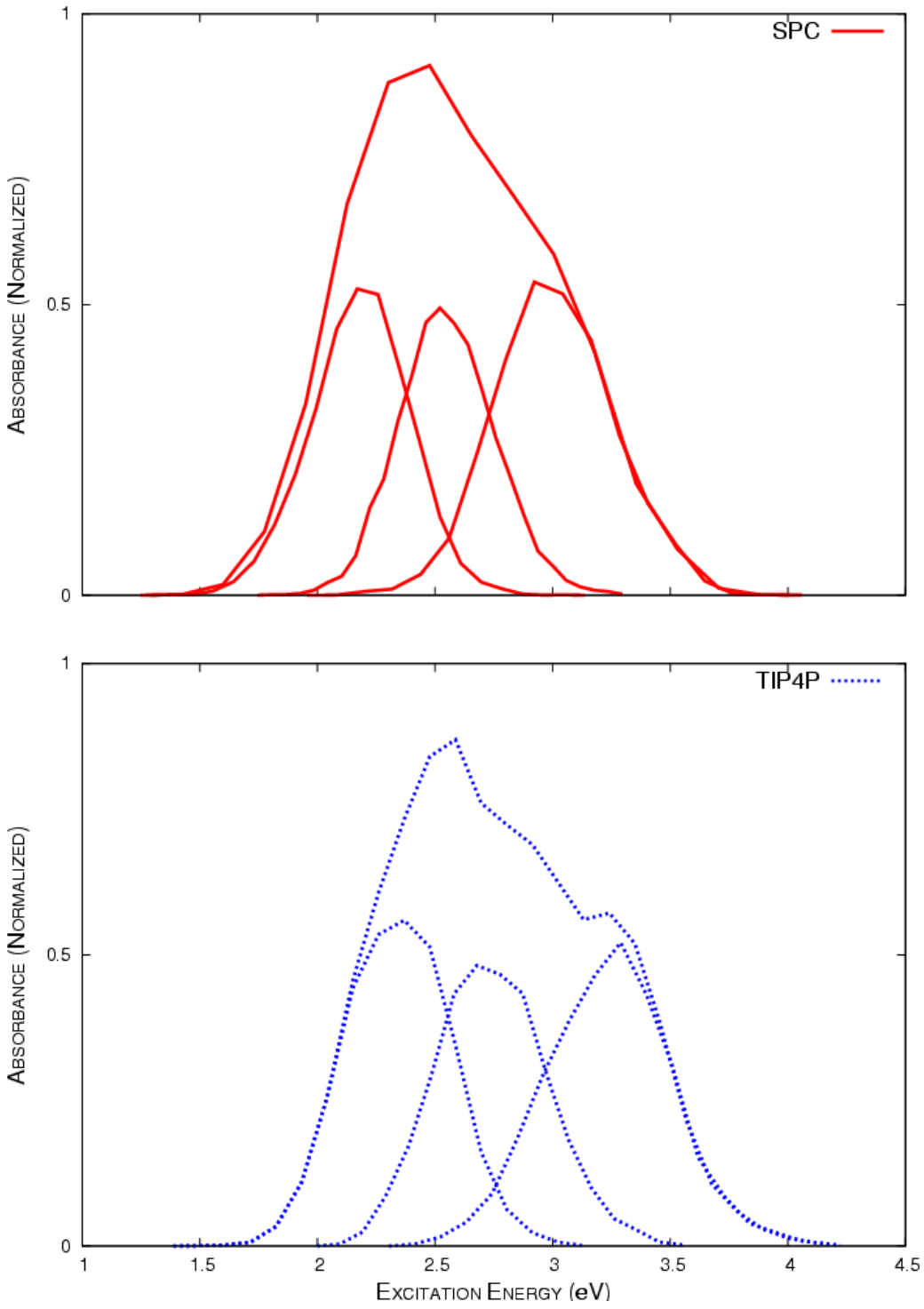

Figure 3.4: Contributions of each of the three $s \rightarrow p$-like transitions to the simulated absorption spectra in Figure 3.3, for (a) the TIP4P water model and (b) the SPC water model.

Experimental investigations, on the other hand, have had ambiguous and contradictory results in trying to selectively excite and monitor specific *p*-like states, leading to speculation that these states interconvert much more rapidly[54, 56, 58, 61, 104]. The dynamics of the solvent cavity are determined by both the solvent motion and its interaction with the electron. The pseudopotential is the same as that used by Rossky, and variations in the classical solvent model in the current simulations result in only minor changes to the solvent dynamics – not enough to result in dramatic variations in cavity interconversion rates. Figure 3.5 shows the cumulative probability distribution functions for interconversion between *p* states.

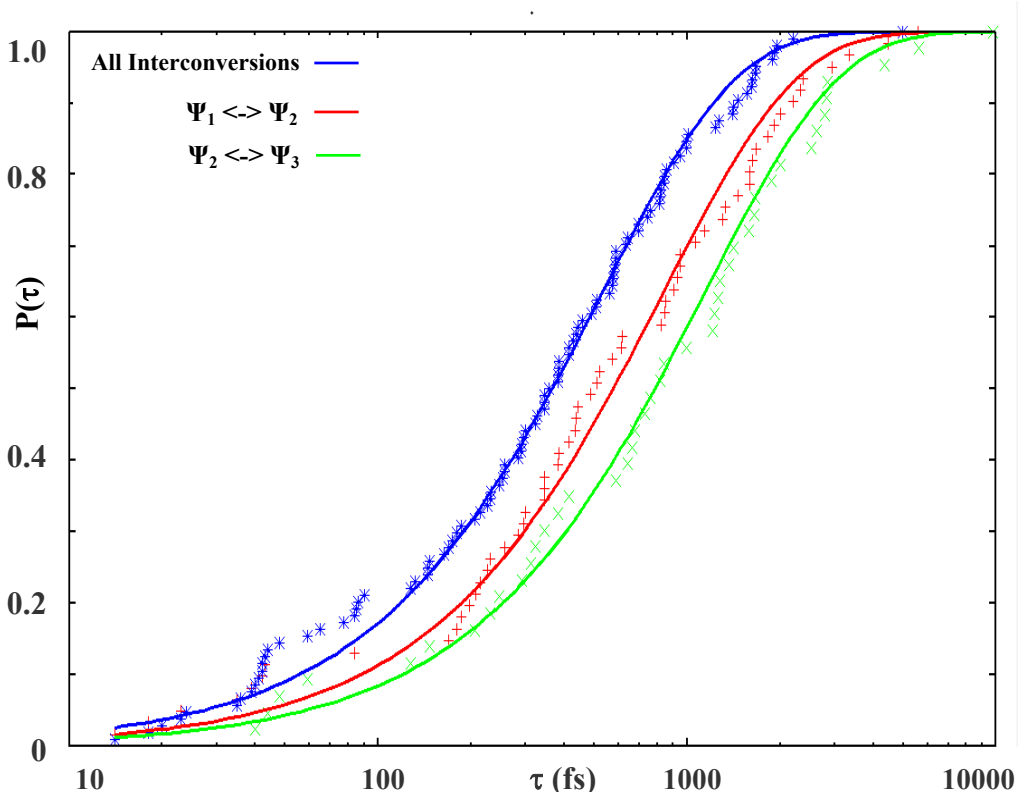

Figure 3.5: Cumulative probability distribution functions for the interconversion rates between *p* states. The lowest lying *p* state is denoted as Ψ_1, the second (intermediate) *p* state is denoted as Ψ_2, and the highest energy *p* state is denoted as Ψ_3. Interconversion rates between the p states are denoted as Ψ_x<-> Ψ_{x+1}.

The distribution of interconversion times are fit well by an exponential distribution. The middle of the three *p*-like states exchanges with the lowest lying *p*-like state with a characteristic time of τ_{12} = 830 fs, and with the highest *p*-like state with a characteristic time of τ_{23} = 1130 fs. The exchanges happen with a characteristic time of τ = 530 fs, when the identity of the swapped states is neglected. These characteristic times were obtained by least-squares fitting to the cumulative distribution functions shown in Figure 3.5.

3.4 Conclusion

The effects of two different rigid, nonpolarizable water models on the physical properties of a hydrated electron have been studied. The SPC and TIP4P water models do result in quantitatively different properties for the hydrated electron. In general, the hydrated electron is slightly better described when solvated with TIP4P water than with SPC water, at least when the Rossky pseudopontetial is used. Neither model results in a truly accurate model of the hydrated electron, however. For example, the electron diffuses about 13% faster in TIP4P water than in SPC water, although the experimental diffusion rate is roughly three times larger. Likewise, the electron's ground state energy is 0.20 eV lower in TIP4P water than in SPC water, but the physical electron is another 0.5 eV more stable. The simulated absorption spectrum, known to be blue-shifted with the Rossky pseudopotential, is blue-shifted more in TIP4P than SPC, while the shape of the simulated absorption spectrum is slightly better (more asymmetric with a high-energy tail) in TIP4P water.

The TIP4P water model provides a more realistic description of the geometric and electrostatic properties of water, including the bond length, bond angle, and average liquid-state dipole moment, than does the SPC model. It also generally provides a better description of the structure and dynamics of liquid water. It is satisfying then, and perhaps not too surprising that the TIP4P water model provides a somewhat more realistic environment for the hydrated electron, in that it more closely resembles the ab initio water with which the Rossky pseudopotential was parameterized[51] and provides more realistic solvent structure and fluctuations. But substantial errors remain in both the energetics and the dynamics of the simulated hydrated electron.

It is likely that the rigidity and the non-polarizability of the SPC and TIP4P water models are responsible for much of the remaining errors. The solvent molecules themselves move on time scales such that a rigid (i.e. mean-field) approximation of the nearby covalent bonds is an accurate approximation, but the electron can easily adapt on the scale of bond vibration, and would diffuse faster in a flexible solvent model. Likewise, the mean-field polarization built into both the solvent models (via the enhanced but constant dipole moment) and the electron-water pseudopotential is quite approximate. It ignores both the anisotropic geometry of the system, as well as the many-body nature of the electrostatic polarization. Implementation of a fully polarizable model could be expected to further stabilize the ground state of the electron (although this is dependent on errors in the mean-field polarization in Eq. (1), which would not be

needed in a pseudopotential for interaction between an electron and polarizable water).

One should not expect, however, that an ever-improving series of classical water models (and pseudopotentials) should eventually converge to an arbitrarily accurate model for the hydrated electron, at least in an adiabatic quantum-classical dynamics simulation. Quantum dynamics, including excited states and quantum mechanical treatment of the solvent may be necessary for a truly quantitative and predictive simulation. Nonetheless, we expect that by carefully decoupling the various features of the solvent model (geometry, rigidity, polarizability) and examining their effects in isolation, it should be possible to understand the origins and the limitations of quantum-classical models of electron solvation. The present work has demonstrated that the geometry of the classical model has a noticeable effect on the properties of the water-electron system, although the effects are relatively small compared to the difference with experiment. The effects of water model rigidity and polarization will be explored in future work.

CHAPTER FOUR
MIXED QUANTUM-CLASSICAL STUDY OF A HYDRATED ELECTRON: I. EFFECTS OF WATER POLARIZATION

4.1 Introduction

Hydrated electrons play a significant role in a variety of biological and chemical processes. To better understand the properties and dynamics of hydrated electrons, extensive theoretical and experimental studies have been conducted on the behavior of a single electron in water[45, 57, 64]. As the smallest quantum mechanical solute, a hydrated electron has given significant insight into the behavior of polar liquids such as water[45, 46].

A variety of water models have been used to study hydrated electrons in the past, ranging from rigid, nonpolarizable models (SPC)[18] to flexible models (SPC/Flex)[67] and polarizable models (pTIP4P)[72-74]. A flexible version of the simple point-charge (SPC/Flex) water model was used by Rossky *et al.* to study the adiabatic and nonadiabatic dynamics of a hydrated electron[50, 51, 95, 96]. Staib and Borgis examined the shape fluctuation and diffusion of an electron solvated by a polarizable version of the four-point transferable intermolecular potential[70] water (pTIP4P), using the floating spherical Gaussian orbital (FSGO) method[97].

Aremu-Cole and Stuart studied theoretically, the role of water geometries on the physical properties of a hydrated electron. The structural, energetic, and dynamical properties of a hydrated electron solvated by SPC and TIP4P water models were observed. Both models used in their comparisons were rigid, nonpolarizable models. It was found that the geometrical differences in the two

water models indeed affected the dynamics of a hydrated electron. Although the differences were small, they were statistically significant. The calculated ground state absorption spectrum is one of the key quantities discussed in these studies, and is repeatedly found to be blue-shifted by 0.5–0.7 eV from the experimental absorption peak.

The goal of this work is to theoretically study the energetics and dynamics of the hydrated electron using a polarizable and nonpolarizable water model. The effect of a polarizable fluctuating charge TIP4P-FQ[71] water model and TIP4P[70] water models on the energetics and dynamics of the solvated electron is analyzed. From prior studies, water models such as TIP4P-FQ and SPC-FQ[71], that explicitly account for polarization have shown tremendous improvements in both the gas and liquid phase properties of bulk water. Properties such as diffusion coefficient, radial distribution functions and dielectric constant calculated using polarizable water models better represent experimental data.

Fluctuating charge models allow charges within the system to evolve as dynamical variables, by combining the electronegativity equalization (EE)[105] and the extended Langrangian[17, 87, 106, 107] methods. Using these methods, charges within a solvent molecule respond to changes in their local environment. This approach is superior to the use of fixed charge models because atoms and molecules experience realistic interactions with their local environments.

In section II, we discuss the details of our simulations, and the pseudopotential used for the electron-water interaction. In section III, we present and discuss the properties of the hydrated electron when solvated by both

polarizable and nonpolarizable water models. Conclusions are presented in section IV.

4.2 Computational details

A. Potential details

Charges, q, are given a fictitious mass, and the charge-charge interaction potential is described by equation (1),

$$U(q,r) = \sum_{i=1}^{Nmol} \sum_{\alpha=1}^{Natoms} [E_\alpha(q_\alpha)] + \sum_{i\alpha<j\beta} J_{\alpha\beta}(r_{i\alpha j\beta}) q_{i\alpha} q_{j\beta} + \sum_{i\alpha<j\beta} V(r_{i\alpha j\beta}). \quad (1)$$

The distance between atom α on molecule i and atom by β on molecule j is $r_{\alpha,\beta}$. Coulomb interactions for the charges are described by the second sum in equation (1), and non-Coulombic interactions are described by the third term, $V(r_{i\alpha j\beta})$[71]. The energy of a system with N_{mol} molecules containing N_{atoms} atoms[71] is represented by $U(q,r)$. The first term in $U(q,r)$, is the energy required to create a partial charge on any atom in the system and this energy is defined as,

$$E_\alpha(q_\alpha) = E_\alpha(0) + \tilde{\chi}^0_\alpha q_\alpha + 0.5 J^0_{\alpha\alpha} q^2_\alpha. \quad (2)$$

The Mulliken electronegativity is described by $\tilde{\chi}^0_\alpha$, and the hardness of the electronegativity of an isolated atom is given by $J^0_{\alpha\alpha}/2$. The calculation of $J_{\alpha\beta}$ is described in detail in Ref. [71], and is also described by Rappe *et al*[108].

In our simulations the overall charge of each molecule is constrained to be neutral; therefore the overall electronegativity of each atomic site within any given molecule is equal. Charge neutrality constraints are enforced using the

method of undetermined Lagrangian multipliers[71], and the motion of charges is governed by the following equation of motion,

$$M_q \ddot{q}_{i\alpha} = -\frac{1}{N_{atom}} \sum_{\beta=1}^{Natom} \left(\tilde{\chi}_{i\alpha} - \tilde{\chi}_{i\beta} \right), \tag{3}$$

where $\tilde{\chi}_{i\alpha} \equiv -\frac{\partial V}{\partial q_{i\alpha}}$, is the instantaneous electronegativity at any given atomic site, within the molecule, and

$$-\frac{1}{Natom} \sum_{\beta=1}^{Natom} -\tilde{\chi}_{i\beta} \tag{4}$$

is the average electronegativity of the molecule. The charge mass defined as M_q, is a non-physical quantity, taken to have a value of 6.0×10^{-5} (ps^2 kcal)/ (e^2 mol)[71]. Using equation (3), new charges can be calculated for all charged interaction sites, as new positions are generated. Just as positions are integrated at every timestep, charges are integrated using the velocity Verlet algorithm and new charges are calculated with every new configuration generated.

The water-electron interactions are described in these simulations via a modified Rossky and Schnitker electron-water pseudopotential[51]. Polarization is no longer treated implicitly as a mean-field potential in the pseudopotential; it is now treated explicitly via polarization of the solvent molecules. The mean-field polarization term is eliminated from the original electron-water pseudopotential, and the new electron–water pseudopotential can be written as

$$V_{ps}(\mathbf{r}) = \sum_i S(|\mathbf{r} - \mathbf{r}_i|) \frac{-q_i}{|\mathbf{r} - \mathbf{r}_i|} + \sum_i \sum_j B_j^{(i)} r^{n_j^{(i)}} e^{-\rho_j^{(i)} |\mathbf{r} - \mathbf{r}_i|}, \tag{5}$$

where the first sum represents the electrostatic interactions, and runs over all interaction sites i with position $\mathbf{r}_i$ and charge q_i. $S(r)$ is a cubic spline that

smoothly turns off the electrostatic interaction inside a cutoff distance r_u, in order to avoid singularities when the electron interacts with a positive nucleus[51]. This cutoff function is one at distances beyond r_u = 0.4 Å for hydrogen atoms and 0 Å for the M site (TIP4P-FQ). The final term represents the core repulsion potential arising from a double-ζ basis set of Slater orbitals. For the TIP4P-FQ water model, these Slater orbitals are centered on the atomic nuclei, with no orbitals residing on the TIP4P M site. The values of the constants B, n, and r that characterize this effective interaction with the water pseudo-wavefunction can be found in the original description of the pseudopotential[51, 95].

The water–water interactions are described via a potential that is a combination of a 12-6 Lennard-Jones potential, electrostatic interactions for both the atoms and charges, and the gas phase energy. The water-water interaction potential is described as follows,

$$U_{\text{int}} = \sum_{i<j} 4\varepsilon \left[\left(\frac{\sigma}{r_{ij}} \right)^{12} - \left(\frac{\sigma}{r_{ij}} \right)^{6} \right] + \sum_{i<j} \left(\frac{q_i q_j}{r_{ij}} \right) + \sum_i \left[\tilde{\chi}_i^0 q_i + \frac{1}{2} \sum_j J_{ij}(r_{ij}) q_i q_j \right] \quad (6)$$

where the Lennard-Jones ε and σ parameters are 0.2862 kcal/mol and 3.159 Å, respectively and acts only on the oxygen atoms[18, 70], and the second and third terms are electrostatic terms, previously described in equation (1).

B. Simulation details

A mixed quantum-classical simulation study of one electron solvated by 200 TIP4P-FQ water molecules was executed, at constant volume in a cubic box of length 18.17 Å. Periodic boundary conditions were used, with the minimum

image convention[1]. The system was equilibrated for 98 ps at a temperature of 298±10 K using the Andersen thermostat[17] with a variable resampling interval of 20-50 fs.

After equilibration, charge velocities were rescaled if charge temperatures defined as qT, became larger than 8 K, and atomic degrees of freedom are thermostatted with the Andersen thermostat at every 200 fs. A 50 ps dynamics simulation was performed after the equilibration period and all property averages were collected during this time.

The velocity Verlet algorithm[109] was used to integrate the dynamics with a timestep of 1 fs, and the RATTLE algorithm[93] was used to satisfy the rigid bond constraints of the TIP4P-FQ water model.

In the mixed quantum-classical system, the time evolution is treated within the Born-Oppenheimer approximation, with the quantum electron moving adiabatically on the ground state electronic surface. This ground state surface is obtained by solving Schrödinger's equation at every timestep on a spatial grid of 16^3 grid points using an iterative block Lanczos scheme[101]. The solvent evolves under the classical forces due to the gradient of the water–water potential, as well as the quantum (Hellman-Feynman) force[52] due to the electron.

4.3 Results

The properties of the hydrated electron have been studied using a polarizable, fluctuating charge water model, TIP4P-FQ. The structure (size) of the electron, its energetics, and its mobility are discussed below, and compared to

two previous studies; the first, a study of a hydrated electron using a flexible nonpolarizable water model, SPC/FLEX by Rossky *et al*[95, 101], and the second is a study of a hydrated electron solvated by two rigid nonpolarizable water models by Aremu-Cole and Stuart[110].

The average radius of gyration is used as a measure of the size of the hydrated electron. Comparing the width of the distribution in Figure 4.1 the effect of the solvent polarizability on the size of the electron can be analyzed. When we solvate the electron using the polarizable TIP4P-FQ water model, we observe that the size of the electron becomes smaller than had been previously documented using the TIP4P water model. Figure 4.1 shows the distribution of the radius of gyration obtained from solvating an electron with both the TIP4P-FQ and TIP4P water molecules.

We found the average (and standard deviation of the) radius of gyration to be 2.35(0.02) Å. Average radius of gyration values calculated using the SPC and TIP4P water models yielded values of 2.1(0.2) Å, and 2.0(0.1) Å, respectively.

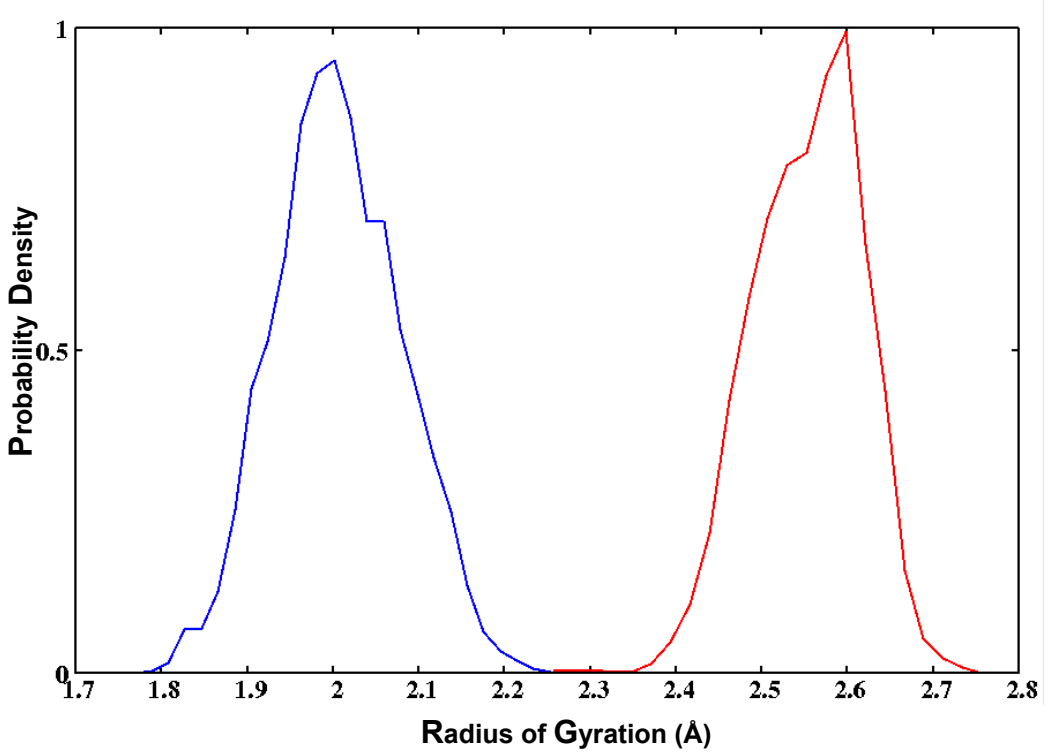

Figure 4.1: Normalized probability density function for the radius of gyration for an electron solvated by TIP4P-FQ water (red line) and TIP4P water (blue line).

At equilibrium the ground-state hydrated electron occupies an approximately spherical cavity, while the first three excited states have *p*-like geometry[53, 101]. A time series of the energies of these four states is shown in Figure 4.2.

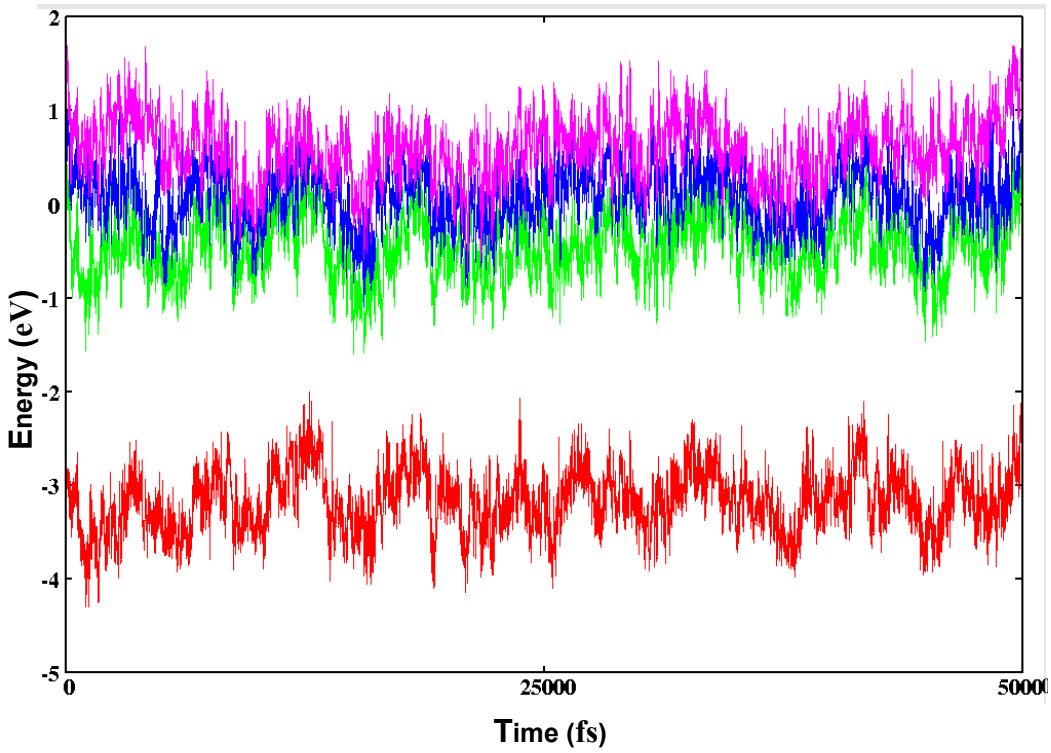

Figure 4.2: Energy (eV) versus time (fs) plots for the electronic energies of a hydrated electron solvated by TIP4P-FQ water molecules. The red line represents the ground state (*s*-like) and the first three excited states (*p*-like) of a hydrated electron are represented by the green, blue and purple lines. The lowest lying *p*-like state is represented by the green line, the blue line represents the second excited state energy, and the purple line represents the highest energy *p*-like state.

Average eigenenergy values have been calculated for each of the energy trajectories in Figure 4.2, and these values are reported in Table 4.1. The ground state energy -3.18 ± 0.3 eV is comparable to the experimental value of -3.32 eV (Ref. [100]). When compared to the calculated average ground state eigenenergies obtained from the TIP4P water models, 2.79 ± 0.3 eV[110], the ground state energy of the electron in the TIP4P –FQ model is more stable and better represents the experimental value.

Energy States	TIP4P-FQ Energies (eV)	TIP4P Energies (eV)
Ground state energy	-3.18 ± 0.01	-2.77 ± 0.02
First excited state	-0.46 ± 0.02	-0.43 ± 0.02
Second excited state	0.06 ± 0.01	-0.03 ± 0.01
Third excited state	0.52 ± 0.01	0.45 ± 0.02

Table 4.1: Average energies and standard deviations of the electronic energy states of a hydrated electron.

The *p*-like states in the TIP4P-FQ water model are split by 0.98 ± 0.03 eV on average. The splitting of the *p*-like energies is broader using the TIP4P-FQ water model, than all three values previously reported using the SPC/FLEX[57], SPC and TIP4P water models[110]. We find that the first three excited states using TIP4P-FQ is 10 % broader than the splitting observed using TIP4P. The average splitting value obtained using TIP4P was 0.89 eV ± 0.03. Cumulative distribution functions have been calculated and are shown in Figure 4.3. The cumulative distributions clearly show the energetic shifts due to the solvent model.

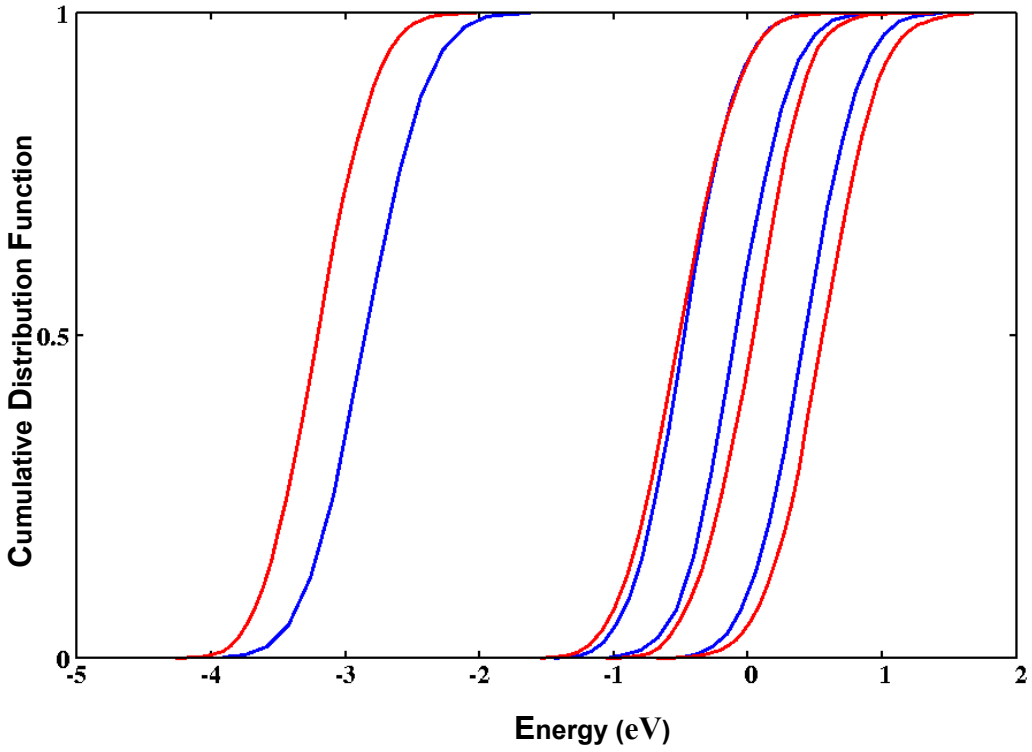

Figure 4.3: Normalized cumulative distribution functions for the energy levels associated with the electron. The red line represents the solvation using TIP4P-FQ water model and the blue line represent solvation using TIP4P water model.

The stabilization of the ground state energy is significant, as well as the destabilization of the higher energy *p*-states using TIP4P-FQ water. A simulated absorption spectrum was calculated from the energy values depicted in Figure 4.3. The calculated absorption spectrum of the electron solvated by TIP4P-FQ water molecules continues to be blue-shifted along with previously calculated data [57, 96, 110]. In our case, the magnitude of the blue-shift is more severe in comparison to previously observed data. Using the TIP4P-FQ model, the maximum peak of the spectrum obtained is at 2.8 eV and a full width at half-maximum (FWHM) is 1.34 eV, whereas with the nonpolarizable TIP4P water model values of 2.6eV

(maximum) and 1.28 eV (FWHM) were calculated. Please refer to Section 3.3. The experimental maximum value is reported as 1.7 eV and the FWHM is reported as 0.8 eV[103]. From these data the calculated absorption spectrum using both water models, is much broader than the experimental spectrum, and surprisingly the nonpolarizable TIP4P water model is better representative of the experimental data than the polarizable TIP4P-FQ water model.

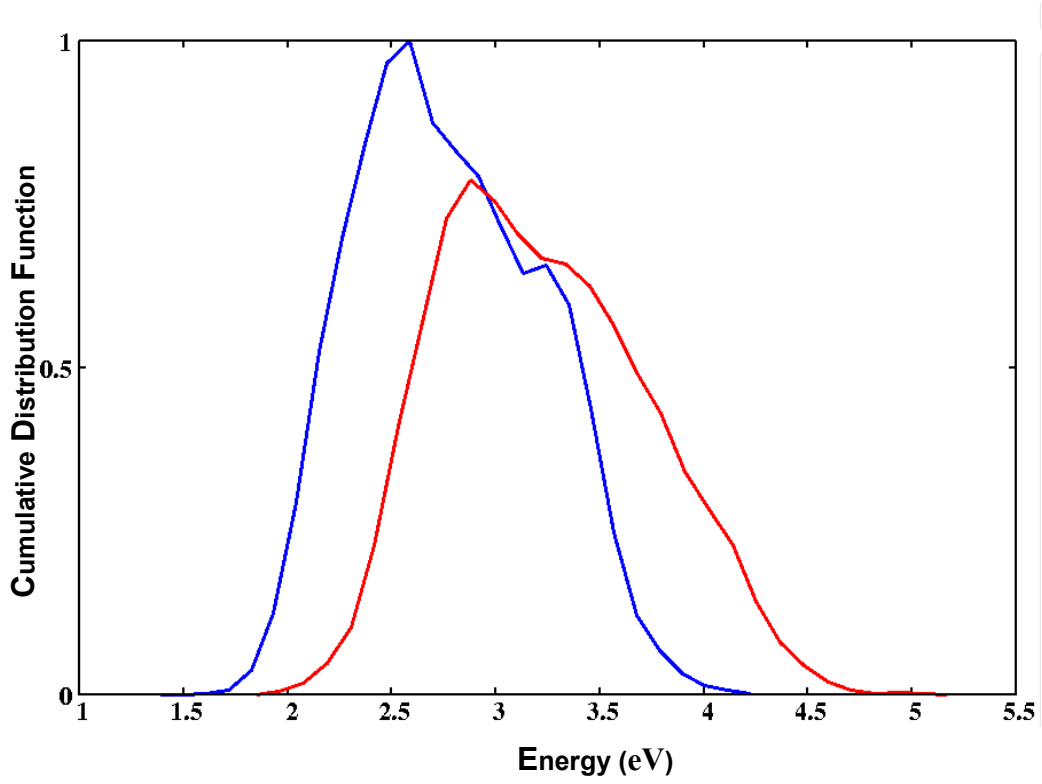

Figure 4.4: Simulated absorption spectra for the hydrated electron in TIP4P-FQ (red line) and TIP4P (blue line) water models.

4.4 Conclusion

The effects of a polarizable water model on the physical properties of a hydrated electron have been studied. The TIP4P-FQ water model provides a

more realistic description of the geometric and electrostatic properties of water, including the bond length, bond angle, and average gas-phase and liquid-phase dipole moments. It also generally provides a better description of the structure and dynamics of liquid water, because charges respond to perturbation, and move in response to their local environments.

Several properties of the hydrated electron were considered. among these are the eigenenergy of the ground state, and the three first excited states. Comparing average theoretically calculated energies of the ground state absorption spectrum; the polarizable TIP4P-FQ water model has shown dramatic improvements in comparison to both the SPC and TIP4P models. There is a significant stabilization in the ground state energy.

However, there have been several problems theoretically reproducing experimentally calculated properties of the hydrated electron. We had hoped that including polarization explicitly through solvent molecules, rather than using the approximate mean field polarization term in the Rossky-Schnitker electron water pseudopotential would help reduce the blue-shifting of the absorption spectrum relative to experiment. Since the TIP4P-FQ water model provides a more realistic description of the geometric and electrostatic properties of water, and it also generally provides a better description of the structure and dynamics of liquid water, we anticipated it would provide a more realistic solvent structure and fluctuations of the energies of a hydrated electron. But substantial errors remain in the energetics of the simulated hydrated electron.

In agreement with our previous study, we observe that the choice of water models significantly affects the theoretical properties of a hydrated electron. It is obvious from this study and the previous ones that the geometries and electrostatic treatments of water models will significantly affect energetic and dynamics of the hydrated electron.

After several analysis of solvent effects on the energetics and dynamics of the water models, we can certainly say that the choice of water models play a significant role in the energetic, structural and dynamic data obtained from simulation studies. We recommend the use of polarizable water model, TIP4P-FQ in conjunction with a reparameterization of the Rossky and Schnitker electron-water pseudopotential. There is a strong indication that the electron-water pseudopotential's treatment of the core repulsion as seen in Section 3.2 A, is not sufficient to describe the solvent electron interactions.

CHAPTER FIVE
CONCLUSION

The effect of Berendsen, Langevin, Velocity rescaling and Andersen temperature control algorithms, on the dynamic behavior of liquid water has been studied. The partitioning of each system's energy between the rotational and translational degrees of freedom, and how this differs for different thermostats, were elucidated. The effects of any violations of equipartition were also considered.

We found that the use of deterministic thermostats such the Berendsen and velocity rescaling thermostats have inherent problems associated with them. Without modifications such as periodically removing center of mass motions, and performing infrequent rescaling, these thermostats will severally dampen the internal energies, and extremely increase the linear momentums of atoms in the system. We recommend that for each simulation the choice of thermostat should depend on the experiment and data been collected. Keeping in mind that as translational energy increases and rotational energy decreases the physical meaning of the system of study begins to break down.

Our primary observation is that the flying ice cube effect is not limited to the velocity rescaling thermostat. This phenomenon also occurs in the Berendsen thermostat, and should be expected to occur in any thermostat that performs a deterministic, rather than stochastic, perturbation of atomic velocities in a way that depends on the system temperature. On the other hand, we confirm that stochastic thermostats such as the Andersen and Langevin algorithms correctly

bring the rotational and translational subsystems into thermal equilibrium, as should occur for proper equilibration in the canonical ensembles.

In Chapters 3 and 4, the effects of two different rigid, nonpolarizable water models and a polarizable water model on the physical properties of a hydrated electron have been studied. We find that all the models used inaccurately describe the hydrated electron. For instance, the simulated absorption spectrum, known to be blue-shifted with the Rossky pseudopotential, is even more blue-shifted as we attempt to improve on the type of water model used in our simulations. In Chapter 3 we thoroughly compared the effects of geometry on the properties of the hydrated electron. We used SPC, a simple point charge model and TIP4P, a model that is parameterized with correct bond length, and angles of water. . The SPC and TIP4P water models do result in quantitatively different properties for the hydrated electron. In general, the hydrated electron is slightly better described when solvated with TIP4P water than with SPC water, at least when the Rossky pseudopontetial is used. Neither model results in a truly accurate model of the hydrated electron, however. For example, the electron diffuses about 13% faster in TIP4P water than in SPC water, although the experimental diffusion rate is roughly three times larger. Likewise, the electron's ground state energy is 0.20 eV lower in TIP4P water than in SPC water, but the physical electron is another 0.5 eV more stable. The simulated absorption spectrum, known to be blue-shifted with the Rossky pseudopotential, is even more blue-shifted in TIP4P than SPC, while the shape of the simulated absorption

spectrum is slightly better (more asymmetric with a high-energy tail) in TIP4P water.

Calculated properties such as ground state average eigenenergies, and shape of the absorption spectrum, favored the TIP4P model, and it appeared that improving water models might improve simulated results, bringing them in better agreement with experiment.

The effect of a polarizable water model on the physical properties of a hydrated electron was then studied. The TIP4P-FQ water model provides a more realistic description of the geometric and electrostatic properties of water, including the bond length, bond angle, and average gas-phase and liquid-phase dipole moments. It also generally provides a better description of the structure and dynamics of liquid water, because charges respond to perturbation, and move in response to their local environments.

We considered several properties of the hydrated electron. Comparing average theoretically calculated energies of the ground state absorption spectrum; the polarizable TIP4P-FQ water model has shown dramatic improvements in comparison to both the SPC and TIP4P models. We observed a significant stabilization in the ground state energy, but the absorption spectrum continues to be blue-shifted.

We had hoped that including polarization explicitly through solvent molecules, rather than using the approximate mean field polarization term in the Rossky-Schnitker electron water pseudopotential would help reduce the blue-shifting of the absorption spectrum relative to experiment. Unfortunately

theoretically properties continue to differ from experimental properties of a hydrated electron.

From all our simulations we conclude that the choice of water models affects the energetics and dynamics of the water models. We can certainly say that the choice of water models play a significant role in the energetic, structural and dynamic data obtained from simulation studies. We recommend the use of polarizable water model, TIP4P-FQ in conjunction with a reparameterization of the Rossky and Schnitker electron-water pseudopotential. There is a strong indication that the electron- water pseudopotential's treatment of the core repulsion is not sufficient to describe the solvent electron interactions.

CHAPTER SIX
REFERENCES

1. Allen, M. P., and D. J. Tildesley, *Computer Simulation of Liquids*. Clarendon: Oxford, 1987.

2. Rapaport, D. C., *The Art of Molecular Dynamics Simulation*. Cambridge University Press: New York, 1995.

3. Alder, B. J., and T. E. Wainwright Velocity Autocorrelations for Hard Spheres. *Phys. Rev. Lett.* **1967,** 18, 988-990.

4. Burkert, U., and N. L. Allinger, Pitfalls in the use of the torsion angle driving method for the calculation of conformational interconversions. *J. Comput. Chem.* **1982,** 3, 40-46.

5. Burkert, U., and N. L. Allinger, *Molecular Mechanics*. Washington, D.C.: American Chemical Society 1982.

6. Metropolis, N., and S. Ulam, The Monte Carlo Method. *J. Amer. Stat. Assoc.* **1949,** 44, 335-341.

7. Fishman, G. S., *Monte Carlo: Concepts, Algorithms, and Applications*. Springer Verlag: New York, 1995.

8. Fock, V., Bemerkung zum Virialsatz. *Z. Physik* **1930,** 61, 126.

9. Hartree, D. R., *Proc. Cam. Phil. Soc.* **1928,** 24, 89.

10. Hartree, D. R., *Proc. Cam. Phil. Soc.* **1928,** 24, 111.

11. Hartree, D. R., *Proc. Cam. Phil. Soc.* **1928,** 24, 426.

12. Hohenberg, P., and W. Kohn, Inhomogeneous electron gas. *Phys. Rev.* **1964,** 136, B864-B871.

13. Kohn, W., and L. J. Sham, Self-consistent equations including exchange and correlation effects. *Phys. Rev.* **1965,** 140, A1133-A1138.

14. D. A. Case, T. E. C., III, T. Darden, H. Gohlke, R. Luo, K. M. Merz, Jr., A. Onufriev, C. Simmerling, B. Wang and R. Woods, The Amber biomolecular simulation programs. *J . Computat. Chem* **2005,** 26, 1668-1688.

15. Brooks, B. R., R. E. Bruccoleri, B. D. Olafson, D. J. States, S. Swaminathan, and M. Karplus, CHARMM: A program for macromolecular

energy, minimization, and dynamics calculations. *J. Comp. Chem.* **1983,** 4, 187-217.

16. Szabo, A., and N. Ostlund., *Modern Quantum Chemistry*. First Revised ed.; McGraw-Hill, Inc: 1982.

17. Andersen, H. C., Molecular dynamics at constant temperature and/or pressure. *J. Chem. Phys.* **1980,** 72, 2384-2393.

18. Berendsen, H. J. C., J. P. M. Postma, W. F. Van Gusteren, and J. Hermans, *Intermolecular Forces*. Reidel: Dordrecht, 1981; p 331-342.

19. Atkins, P. W., and R.S. Friedman, *Molecular Quantum Mechanics*. 3 ed.; Oxford University Press: New York, NY, 1997.

20. Stillinger, F. H., and A.J. Rahman, Improved simulation of liquid water by molecular dynamics. *J. Chem. Phys.* **1974,** 60, 1545.

21. McCammon, J. A., B. R. Gelin, and M. Karplus, Dynamics of folded proteins. *Nature* **1977,** 267, 585-590.

22. Chandler, D., *Introduction to Modern Statistical Mechanics*. Oxford University Press: New York, NY, 1987.

23. McQuarrie, D., *Statistical Mechanics*. University Science Books: Sausalito, CA, 2000.

24. Schneider, T., and E. Stoll, Molecular-dynamics study of a three-dimensional one-component model for distortive phase transitions *Phys. Rev. B* **1978,** 17, 1302-1322.

25. Kubo, R., The Fluctuation Dissipation Theorem. *Rep. Prog. Phys.* **1966,** 29, 255-284.

26. Ryckaert, J. P., and G. Ciccotti, Introduction of Andersen's demon in the molecular dynamics of systems with constraints. *J. Chem. Phys.* **1983,** 78, 7368-7374.

27. Gear, C. W., *Numerical Initial Value Problems in Ordinary Differential Equations*. Prentice-Hall: Englewood Cliffs, NJ, 1971.

28. Verlet, L., Computer "experiments" on classical fluids. II. Equilibrium correlation functions *Phys. Rev.* **1968,** 165, 201.

29. Verlet, L., Computer ``experiments" on classical fluids: I. Thermodynamical properties of Lennard-Jones molecules. *Phys. Rev.* **1967,** 159, 98.

30. Griffiths, D., *Introduction to Quantum Mechanics*. Prentice Hall: Upper Saddle River, NJ, 1995.

31. Mackey, G., *The Mathematical Foundations of Quantum Mechanics*. Dover Publications: Mineola, NY, 2004.

32. McQuarrie, D., *Quantum Mechanics*. University Science Books: Mill Valey, CA, 1983.

33. Brehm, J. J., and W. J. Mullin, *Introduction to the Structure of Matter: A Course in Modern Physics*. John Wiley and Sons: New York, NY, 1989.

34. Cohen-Tannoudji, C., D. Bernard, and F. Laloe, *Quantum Mechanics*. John Wiley and Sons: New York, NY, 1977; Vol. I and II.

35. Griffiths, D., *Introduction to Quantum Mechanics*. 2 ed.; Prentice Hall: Upper Saddle River, NJ, 2004.

36. Tuvi, I., and Y. B . Band, Modified Born-Oppenheimer basis for nonadiabatic coupling: Application to the vibronic spectrum of HD^+. *J. Chem. Phys.* **1999,** 111, 5808.

37. Esry, B. D., and H. R. Sadeghpour, Adiabatic formulation of heteronuclear hydrogen molecular ion. *Phys. Rev. A* **1999,** 60, 3604.

38. Moss, R. E., and L. Valenzano, Adiabatic and non-adiabatic corrections to properties of the hydrogen molecular cation and its isotopomers: Dissociation energies and bond lengths *Mol. Phys.* **2002,** 100, 649.

39. Moss, R. E., Calculations for vibration-rotation levels of HD , in particular for high N. *Mol. Phys.* **1993,** 78, 371.

40. Wolniewicz, L., and J. D. Poll, On the higher vibration-rotational levels of HD^+ and H_2 *Molec. Phys.* **1986,** 59, 953.

41. Wolniewicz, L., and J. D. Poll, The vibration–rotational energies of the hydrogen molecular ion HD^+. *J. Chem. Phys.* **1980,** 73, 6225.

42. Tully, J. C., Mixed quantum-classical dynamics. *Faraday Discuss.,* **1998,** 110, 407-419.

43. McLachlan, A. D., The wave functions of electronically degenerate states. *Mol. Phys* **1961,** 4, 417-423.

44. Tully, J. C., and R. K. Preston, Trajectory surface hopping approach to nonadiabatic molecular collisions: The reaction of H^+ with D_2 *J. Chem. Phys.* **1971,** 55, 562-572.

45. Mosyak, A. A., O.V. Prezhdo, and P.J. Rossky, Solvation dynamics of an excess electron in methanol and water. *J. Chem. Phys.* **1998,** 109, 6390.

46. Yang, C., K. F. Wong, S. Skaf, and P. J.Rossky, Instantaneous normal mode analysis of hydrated electron solvation dynamics. *J. Chem. Phys.* **2001,** 114, 3598.

47. Long, F. H., H. Lu and K.B. Eisenthal, Femtosecond studies of the presolvated electron: An excited state of the solvated electron? . *Phys. Rev. Lett.* **1990** 64 1469.

48. Migus, A., Y. Gauduel, J. L. Martin and A. Antonetti, Excess electrons in liquid water: First evidence of a prehydrated state with femtosecond lifetime. *Phys. Rev. Lett.* **1987,** 58, 1559.

49. Del Buono, G. S., P. J. Rossky, and T. H. Murphrey, Diffusive transport of the hydrated electron: A pseudoclassical model. *J. Phys. Chem.* **1992,** 96, 7761-7769.

50. Motakabbir, K. A., Schnitker, J., Rossky, P.J. , A comparison of classical and quantum analyses of electron localization sites in liquid water. *J. Chem. Phys.* **1992,** 97, 2055.

51. Schnitker, J., and P. J. Rossky, An electron-water pseudopotential for condensed phase simulation. *J. Chem. Phys.* **1986,** 86, 3462.

52. Webster, F. A., P.J. Rossky, and R. A. Friesner, Nonadiabatic processes in condensed matter: Semi-classical theory and implementation. *Comput. Phys. Commun.* **1991,** 63, 494.

53. Borgis, D., and S. Bratos, Theoretical description of the hydrated electron. Shape and spectroscopic properties of the cavity containing the excess electron. *J. Mol. Struct.* **1997,** 436 - 37, p. 537-541.

54. Yokoyama, K., Silva, C., Son, D. H., Walhout, P.K., and P.F. Barbara, Detailed investigation of the femtosecond pump-probe spectroscopy of the hydrated electron. *J. Phys. Chem. A* **1998,** 102, 6957.

55. Yu, J., and M. Berg, Local anisotropy and structural and phonon dynamics of permanganate (MnO^{4-}) in glassy and liquid lithium chloride hexahydrate by ultrafast transient hole burning. *J. Phys. Chem.* **1993,** 97, 1758.

56. Reid, P. J., C. Silva, P.K. Walhout, and P.F. Barbara, Femtosecond absorption anisotropy of the aqueous solvated electron. *Chem. Phys. Lett.* **1994,** 228, 658-664.

57. Schwartz, B. J., and P.J. Rossky, Pump-probe spectroscopy of the hydrated electron: A QMD simulation. *J. Chem. Phys.* **1994,** 101, 6917.

58. Cavanaugh, M. C., I. B. Martini, and B. J. Schwartz, Revisiting the pump–probe polarized transient hole-burning of the hydrated electron: Is its absorption spectrum inhomogeneously broadened? *Chem phys Lett* **2004,** 396, 359-366.

59. Baltuska, A., Emde, M. F., Pshenichnikov, M. S., and D. A. Wiersma, Early-time dynamics of the photoexcited hydrated electron. *J. Phys. Chem. A* **1999,** 103, 10065-82.

60. Tauber, M. J., and R.A. Mathies, Resonance Raman spectra and vibronic analysis of the aqueous solvated electron. *Chem phys Lett* **2002,** 354, 518.

61. Tauber, M. J., and R.A.Mathies, Structure of the aqueous solvated electron from resonance raman spectroscopy: Lessons from isotopic mixtures. *J. Am. Chem. Soc* **2003,** 125, 1394.

62. Mizuno, M., and T. Tahara, Novel resonance Raman enhancement of local structure around solvated electrons in water. *J. Phys. Chem. A* **2001,** 105, 8823-26.

63. Schnitker, J., K. Motakabbir, P.J. Rossky and R. Friesner, A priori calculation of the optical-absorption spectrum of the hydrated electron. *Phys. Rev. Lett* **1988,** 60, 456.

64. Schwartz, B. J., and P.J. Rossky, Aqueous solvation dynamics with a quantum mechanical Solute: Computer simulation studies of the photoexcited hydrated electron. *J. Chem. Phys.* **1994,** 101, 6902.

65. Barnett, R. B., U. Landman, and A. Nitzan, Relaxation dynamics following transition of solvated electrons. *J. Chem. Phys.* **1989,** 90, 4413.

66. Turi, L., and D. Borgis, Analytical investigations of an electron-water molecules pseudopotential. II. Development of a new pair of potential and molecular dynamics simulations. *J. Chem. Phys.* **2002,** 117, 6186.

67. Wu, Y., H. L. Tepper, and G.A. Voth, Flexible simple point charge water model with improved liquid state properties. *J. Chem. Phys.* **2006,** 124, 024503.

68. Kusalik, P. G., and I. M. Svishchev, The spatial structure in liquid water. *Science* **1994,** 265, 1219-1221.

69. Grigera, J. R., An effective pair potential for heavy water. *J. Chem. Phys.* **2001,** 114, 8064-8067.

70. W. L Jorgensen, J. C., J. D. Madura, R.W Impey, and M.L. Klein, Comparison of simple potential functions for simulating liquid water. *J. Chem. Phys* **1983,** 79, 926-935.

71. Rick, S., S. J. Stuart, and B. J. Berne, Dynamical fluctuating charge force fields:Application to liquid water. *J. Chem. Phys.* **1994,** 101, 6141-6156.

72. Sprik, M., Computer simulation of the dynamics of induced polarization fluctuations in water. *J. Phys. Chem.* **1991,** 95, 2283.

73. Sprik, M., and M.L. Klein, A polarizable model for water using distributed charge sites. *J. Chem. Phys.* **1988,** 89, 7556.

74. Sprik, M., M.L. Klein, and K. Watanable, Solvent polarization and hydration of the chlorine anion. *J. Phys. Chem* **1990,** 94, 6483.

75. Mahoney, M. W., and W. L. Jorgensen, A five-site model for liquid water and the reproduction of the density anomaly by rigid, nonpolarizable potential functions. *J. Chem. Phys.* **2000,** 112, 8910-8922.

76. Rick, S. W., A reoptimization of the five-site water potential (TIP5P) for use with Ewald sums. *J. Chem. Phys.* **2004,** 120, 6085-6093.

77. Van Maaren, P. J., and D. Van der Spoel, Molecular dynamics of water with novel shell-model potentials. *J. Phys. Chem. B* **2001,** 105, 2618-2626.

78. Lamoureux, G., E. Harder, I. V. Vorobyov, B. Roux, and A. D. MacKerell Jr. , A polarizable model of water for molecular dynamics simulations of biomolecules. *Chem. Phys. Lett.* **2005,** 418, 241-245.

79. Guillot, B., A reappraisal of what we have learnt during three decades of computer simulations in water. *J. Mol. Liquids* **2002,** 101, 219-260.

80. Halgren, T. A., and W. Damm, Polarizable force fields. *Current Opinion Struct. Biol.* **2001,** 11, 236.

81. Horn, H. W., W. C. Swope, J. W. Pitera, J. D. Madura, T. J. Dick, G. L. Hura, and T. Head-Gordon, Developement of an improved four-site water model for bimolecular simulations: TIP4P-Ew. *J. Chem. Phys.* **2004,** 120, 9665-9678.

82. Abascal, J. L. F., E. Sanz, R. G. Fernandez, and C. Vega, A potential model for the study of ices and amorphous water: TIP4P/Ice. *J. Chem. Phys.* **2005,** 122, 234511.

83. Abascal, J. L. F., and C. Vega, A general purpose model for the condensed phases of water: TIP5P/2005. *J. Chem. Phys.* **2005,** 123, 234505.

84. Stllinger, F. H., and A. Rahman, Improved simulation of liquid water by molecular dynamics. *J. Chem. Phys.* **1974,** 60, 1545-1557.

85. Hoover, W. G., Canonical dynamics: Equilibrium phase-space distributions *Phys. Rev. A* **1985,** 31, 1695.

86. Nosé, S., Constant temperature molecular dynamics. *J. Phys. Condens. Matter* **1990,** 2, SA115-SA119

87. Nosé, S., A molecular dynamics method for simulations in the canonical ensemble *Mol. Phys* **1984,** 52, 255.

88. Harvey, S. C., Tan, R. K.-Z., and T. E. Cheatham III, The flying ice cube: Velocity rescaling in molecular dynamics leads to violation of energy equipartition. *J. Comput. Chem.* **1998,** 19, 726-740.

89. Mark, P., and L. Nilsson Structure and dynamics of liquid water with different long-range interaction truncation and temperature control methods in molecular dynamics simulations. *J. Comput. Chem.* **2002,** 23, 1211-1219.

90. Berendsen, H. J. C., J. R. Grigera, and T. P. Straatsma, The missing term in effective pair potentials. *J. Phys. Chem.* **1987,** 91 6269.

91. Swope, W. C., H. C. Andersen, P. H. Berens and R. Wilson, A computer simulation method for the calculation of equilibrium constants for the formation of physical clusters of molecules: Application to small water clusters. *J. Chem. Phys.* **1982,** 76, 637.

92. Tuckerman, M., Berne, B.J., and G. J. Martyna, Reversible multiple time scale molecular dynamics. *J. Chem. Phys.* **1992,** 97, 1990.

93. Andersen, H. C., Rattle: A "velocity" version of the shake algorithm for molecular dynamics calculations *J. Comput. Phys.* **1983,** 52, 24.

94. Neumann, M., *J. Chem. Phys.* **1986,** 85, 1567.

95. Rossky, P. J., Schnitker, J., The hydrated electron: quantum simulation of structure, spectroscopy, and dynamics. *J. Phys. Chem.* **1988,** 92, 4277.

96. Schnitker, J., Rossky, P. J., Excess electron migration in liquid water. *J. Phys. Chem.* **1989,** 93, 6965-6969.

97. Staib, A., and D. Borgis, Molecular dynamics simulation of an excess charge in water using mobile Gaussian orbitals. *J. Chem. Phys.* **1995,** 103, 2642.

98. Krohn, C. E., P.R. Antoniewicz, and J.C. Thompson, Energetics for photoemission of electrons into NH_3 and H_2O *Surf. Sci.* **1980,** 101, 241.

99. Thompson, J. C., P.R. Antoniewicz, and C.E. Krohn, *Comments Solid State Phys.* **1980,** 9, 223.

100. Coe, J. V., A.D. Earhart, M.H. Cohen, G.J. Hoffman, H.W. Sarkas, and K.H. Bowen, Using cluster studies to approach the electronic structure of bulk

water: Reassessing the vacuum level, conduction band edge, and band gap of water. *J. Chem. Phys.* **1997,** 107, 6023.

101. Schnitker, J., and P. J. Rossky, Quantum simulation study of hydrated electron. *J. Chem. Phys.* **1987,** 86, 3417.

102. Robinson, R., A, and R. H. Stokes *Electrolyte solutions*. 2nd Rev. ed.; Dover Publications: Butterworths, London, 2002.

103. Jou, F.-Y., and G. R. Freeman Temperature and isotope effects on the shape of the optical absorption spectrum of solvated electrons in water. *J. Phys. Chem.* **1979,** 83, 2383.

104. Kimura, Y., Alfano, J.C., Walhout, P.K., and P. F. Barbara, Ultrafast transient absorption spectroscopy of the solvated electron in water. *J. Phys. Chem.* **1994,** 98, 3450.

105. Sanderson, R. T., An interpretation of bond lengths and a classification of bonds *Science* **1951,** 114, 670.

106. Parrinello, M., and A. Rahman, Crystal structure and pair potentials: A molecular-dynamics study. *Phys. Rev. Lett.* **1980,** 45, 1196.

107. Car, R., and M. Parrinello, Unified approach for molecular dynamics and density-functional theory. *Phys. Rev. Lett.* **1985,** 55, 2471.

108. Rappe, A. K., and W. A. Goddard, Charge Equilibration for Molecular Dynamics Simulations. *J. Phys. Chem.* **1991,** 95, 3358.

109. Swope, W., Andersen, H., Berens, P.H., and R. Wilson, A computer simulation method for the calculation of equilibrium constants for the formation of physical clusters of molecules: Application to small water clusters. *J. Chem. Phys.* **1982,** 76, 637.

110. Aremu-Cole, J., and S. J. Stuart, Mixed quantum–classical study of a hydrated electron: I. Effects of water model geometry. *In Prep.* **2007**.